ORNL/TM-5535

Analysis of a Neutron Scattering and Gamma-Ray Production Integral Experiment on Oxygen for Neutron Energies from 1 to 15 MeV

S. N. Cramer
E. M. Oblow

OAK RIDGE NATIONAL LABORATORY
OPERATED BY UNION CARBIDE CORPORATION FOR THE ENERGY RESEARCH AND DEVELOPMENT ADMINISTRATION

DISCLAIMER

Printed in the United States of America. Available from
National Technical Information Service
U.S. Department of Commerce
5285 Port Royal Road, Springfield, Virginia 22161
Price: Printed Copy $4.50; Microfiche $2.25

ORNL/TM-5535

Contract No. W-7405-eng-26

Neutron Physics Division

ANALYSIS OF A NEUTRON SCATTERING AND GAMMA-RAY PRODUCTION INTEGRAL EXPERIMENT ON OXYGEN FOR NEUTRON ENERGIES FROM 1 TO 15 MeV

S. N. Cramer and E. M. Oblow

Manuscript Prepared by Virginia D. Glidewell

This Work Supported by
DEFENSE NUCLEAR AGENCY
Under Subtask PE083

Date Published: September 1976

OAK RIDGE NATIONAL LABORATORY
Oak Ridge, Tennessee 37830
operated by
UNION CARBIDE CORPORATION
for the
ENERGY RESEARCH AND DEVELOPMENT ADMINISTRATION

THIS PAGE

WAS INTENTIONALLY

LEFT BLANK

Table of Contents

THIS PAGE

WAS INTENTIONALLY

LEFT BLANK

Abstract

Monte Carlo calculations were performed to analyze an integral experiment on a liquid oxygen sample to determine the adequacy of the neutron scattering and gamma-ray production data for oxygen. The experimental results included energy- and angular-dependent NE-213 detector count rates and secondary pulse-height spectra for scattered neutrons and gamma rays. The sample was a spherical dewar of liquid oxygen pulsed with a 1- to 20-MeV neutron source. Pulse-height data were unfolded to generate secondary neutron and gamma-ray production spectra as a function of angle in broad incident neutron energy bins. Analysis of all the reported data was based on multigroup Monte Carlo calculations using the MORSE code. Results indicate that the current ENDF/B-IV neutron and gamma-ray production data for oxygen above 1 MeV appear to be in good order. The only major discrepancy uncovered was related to neutron scattering and gamma-ray production from first level inelastic scattering interactions. Calculated results for the production of 6-MeV gamma rays from the 6-MeV first inelastic level in oxygen appear to be low by around 50% at energies above the inelastic threshold. Likewise, calculated secondary neutron spectra for incident neutron energies above 6 MeV are uniformly low at energies corresponding to neutrons having had first level inelastic scattering events in oxygen. Additional deficiencies in the oxygen cross-section data are indicated for inelastic scattering from the cluster of discrete levels in the 12-13 MeV range and for elastic scattering at very small angles at energies above 2 MeV. The size of the inelastic discrepancies are larger than the 20-30% order of error indicated for these cross sections in the ENDF/B-IV uncertainty files for oxygen.

I. Introduction

Calculations of neutron and gamma-ray integral count rates and secondary energy spectra were performed for comparison with the results of an integral measurement on liquid oxygen. The calculations and the experiments were done at Oak Ridge National Laboratory[1,2] as part of The Defense Nuclear Agency data testing program. This effort was designed to test neutron scattering and gamma-ray production data for several nuclides of interest to DNA for incident neutron energies from 1 to 15 MeV. The calculations, experiments, and comparisons presented here are similar to those already completed for carbon[3] and nitrogen.[4] The procedures for the data testing program were outlined in these earlier references in terms of experimental technique, calculational models, and methods of data comparison.

The current experiment consisted of a dewar filled with liquid oxygen pulsed by a collimated beam of neutrons traveling approximately 50 meters from source to sample. NE-213 detectors were used to detect both neutrons and gamma rays scattering from the sample. The detectors were placed outside the flight path of the incident beam at angles with respect to the beam direction of approximately 30, 55, 90, and 125 deg. The data were reduced to neutron and gamma-ray counts as a function of time and reported as counts per incident neutron as a function of incident neutron energy by using time-of-flight considerations. Pulse-height information was also recorded as a function of arrival time so that the differential spectrum of neutrons and gamma rays could be obtained by unfolding techniques as a function of incident neutron energy. Gamma-ray counts induced by neutron interactions in the detector were removed from the experimental data which are reported in Ref. 1.

All calculations used to analyze the experiments were made with the MORSE[5] multigroup Monte Carlo code using coupled neutron-gamma-ray multigroup data from the DNA library[6] processed by the AMPX[7] code system. The results of the analysis are presented in the form of comparisons of the experimental with the calculated results.

The experimental arrangement is described in Section II and the calculational model in Section III. Experimental and calculated results are presented in Section IV followed by a discussion in Section V and conclusions in Section VI.

II. Experimental Arrangements

The ORNL experimental setup is shown in Fig. 1. The Oak Ridge Electron Linear Accelerator (ORELA) was used to create a white pulsed source (12 nsec burst width) from the Be(γ,n) reaction. These neutrons were collimated into a 13.26-cm effective diameter beam and traveled 47.35 meters along a flight path to the scattering sample forming a uniformly distributed mono-directional source at the sample position. The source and flight path are shown in Fig. 2.

The scattering sample consisted of a thin evacuated Pyrex dewar filled with 4.27 liters of liquid oxygen with a density of 1.14 g/cm^3. The unfilled dewar weighed 1256.5 grams and was 22.69 cm in outer diameter. More specifications of the dewar can be found in Ref. 1. The 4.22 cm x 4.65 cm NE-213 detector, used for both neutrons and gamma-ray detection, was placed at four different positions corresponding to angles of 30, 55, 90, and 125 deg with respect to the incident beam direction. The collimated beam was centered on the face of the dewar at an angle of 2 deg with respect to the horizontal line of the detectors. The experimental data consisted of integral count rates and pulse-height spectra for both neutrons and gamma rays at each detector location.

III. Calculational Model

A. Codes and Cross-Section Data

All calculations presented in this report were made with the MORSE[5] multigroup Monte Carlo code using coupled neutron-gamma multigroup data processed by the AMPX[7] code system.

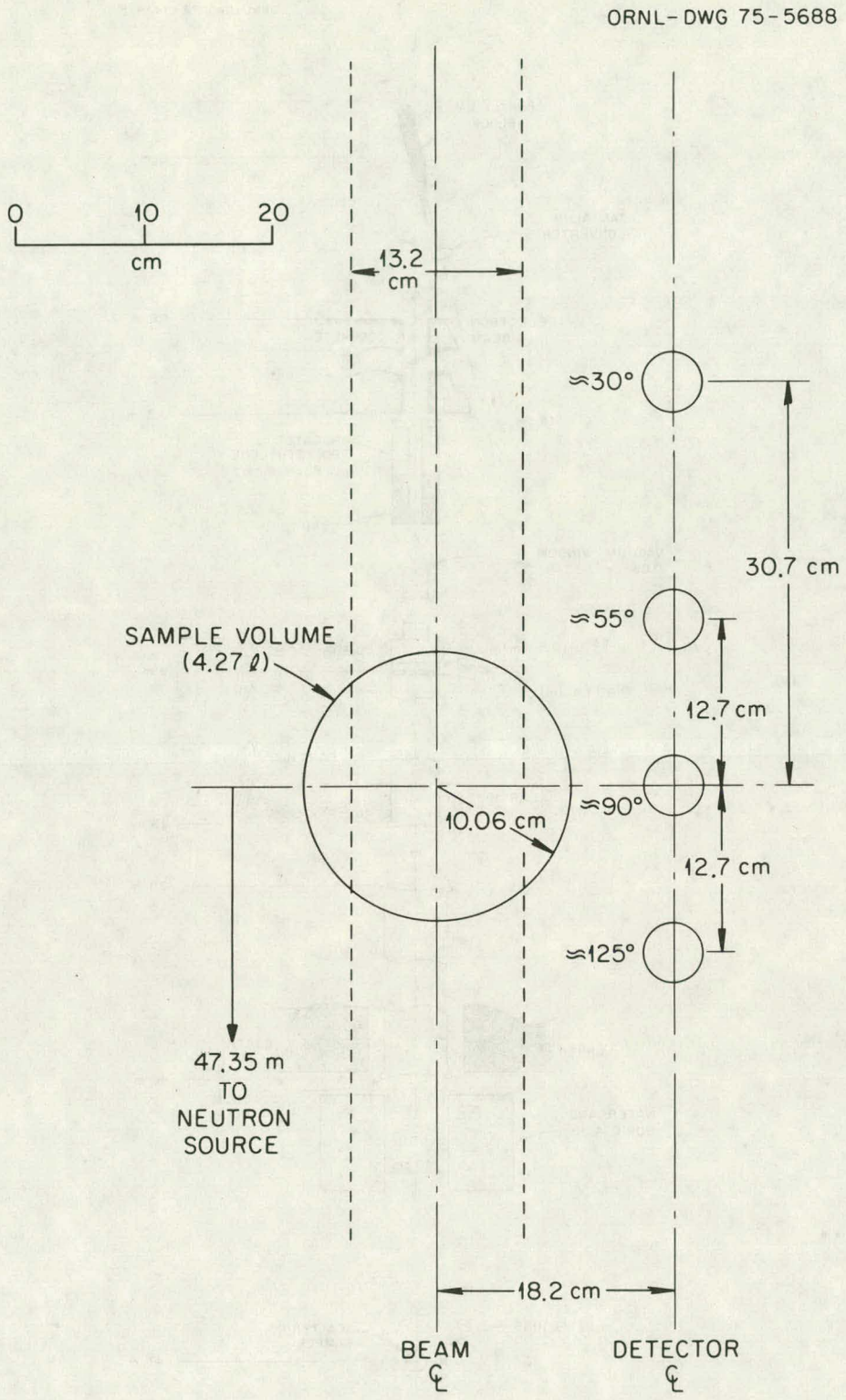

Fig. 1. Top View of Oxygen Dewar and Detectors in ORNL Experiment.

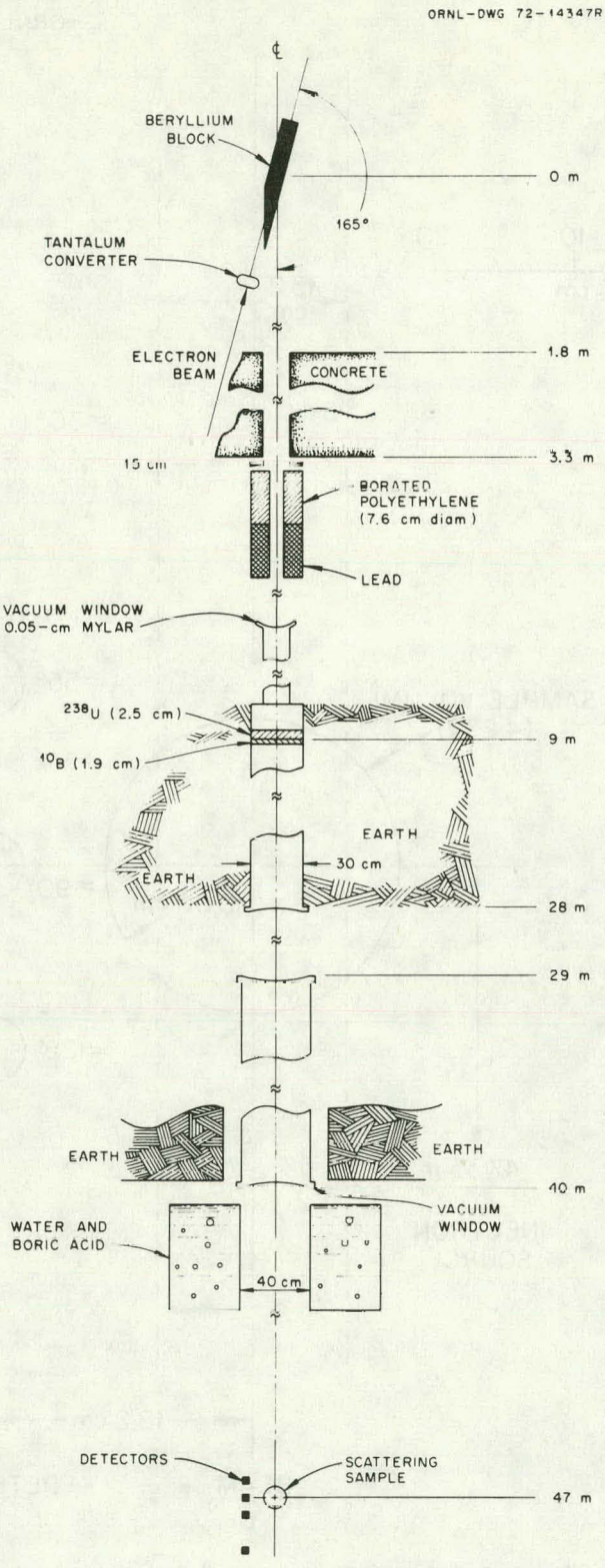

Fig. 2. Neutron Source and Flight Path at ORELA Used for ORNL Integral Experiment.

The oxygen cross-section data set used in the calculations was taken from the DNA MAT 4276 data file (equivalent to ENDF/B-IV). A density of 0.04306 at/barn-cm was used for the liquid oxygen. The Pyrex dewar was mocked up as pure SiO_2 using DNA MAT 4194 silicon data (equivalent to ENDF/B-IV) with density of 0.02325 at/barn-cm and DNA MAT 4276 oxygen data with a density of 0.0465 at/barn-cm.

The cross sections for each case were processed by AMPX into a 103-38 coupled neutron-gamma group structure with a P_7 Legendre expansion and a 1/E weighting function to simulate the incident source spectrum. The cross-section group structure is shown in Table I along with the detector efficiencies. The neutron groups are equally spaced in lethargy between 20 MeV and 300 keV. The calculation was run in the MORSE primary particle mode in which gamma rays are produced utilizing neutron to gamma group transfer probabilities and gamma-ray angular production data.

B. Calculational Procedure

Neutrons and gamma rays were followed from production to detection as a function of space, angle, and time. Neutron histories were started uniformly per unit lethargy from 20 MeV to the lowest energy with reported experimental data. The initial spatial coordinates of the neutrons were determined by selecting x and y uniformly over the 138.1-cm^2 effective cross-sectional area of the neutron beam and placing z at the leading edge of the sample. Neutrons were started straight ahead in the z direction. Gamma rays produced in the sample acquired the position, time, and calculational weight of the neutrons which produced them.

Source neutrons in each energy group were given initial times determined by the time-of-flight of a neutron at the midpoint of each energy group to the leading edge of the sample. Relativistic velocities were used throughout the calculations. The initial times were smeared with a Gaussian approximation of the experimentally determined time spread as follows:

Table I. Energy Group Structure (103 Neutron Groups and 38 Gamma-Ray Groups) and Detector Efficiencies

Group No.	Upper Energy (eV)	Detector Efficiency	Group No.	Upper Energy (eV)	Detector Efficiency
1	2.0000E 07	1.4880E-01	51	3.3652E 06	2.7240E-01
2	1.9300E 07	1.4940E-01	52	3.2474E 06	2.7570E-01
3	1.8624E 07	1.4990E-01	53	3.1337E 06	2.7880E-01
4	1.7972E 07	1.5000E-01	54	3.0239E 06	2.8180E-01
5	1.7342E 07	1.4900E-01	55	2.9180E 06	2.8470E-01
6	1.6735E 07	1.4740E-01	56	2.8159E 06	2.8750E-01
7	1.6149E 07	1.4600E-01	57	2.7173E 06	2.8980E-01
8	1.5584E 07	1.4600E-01	58	2.6221E 06	2.9250E-01
9	1.5038E 07	1.4640E-01	59	2.5303E 06	2.9570E-01
10	1.4511E 07	1.4740E-01	60	2.4417E 06	2.9830E-01
11	1.4003E 07	1.4880E-01	61	2.3562E 06	3.0080E-01
12	1.3513E 07	1.5050E-01	62	2.2737E 06	3.0320E-01
13	1.3040E 07	1.5250E-01	63	2.1941E 06	3.0520E-01
14	1.2583E 07	1.5490E-01	64	2.1172E 06	3.0710E-01
15	1.2142E 07	1.5730E-01	65	2.0431E 06	3.0900E-01
16	1.1717E 07	1.5880E-01	66	1.9715E 06	3.1070E-01
17	1.1307E 07	1.6010E-01	67	1.9025E 06	3.1240E-01
18	1.0911E 07	1.6120E-01	68	1.8359E 06	3.1390E-01
19	1.0529E 07	1.6220E-01	69	1.7716E 06	3.1540E-01
20	1.0160E 07	1.6320E-01	70	1.7096E 06	3.1680E-01
21	9.8044E 06	1.6500E-01	71	1.6497E 06	3.1810E-01
22	9.4611E 06	1.6710E-01	72	1.5919E 06	3.1850E-01
23	9.1298E 06	1.6930E-01	73	1.5362E 06	3.1860E-01
24	8.8101E 06	1.7170E-01	74	1.4833E 06	3.1840E-01
25	8.5016E 05	1.7420E-01	75	1.4305E 06	3.1810E-01
26	8.2039E 06	1.7680E-01	76	1.3804E 06	3.1760E-01
27	7.9166E 06	1.8050E-01	77	1.3321E 06	3.1700E-01
28	7.6391E 06	1.8460E-01	78	1.2854E 06	3.1630E-01
29	7.3719E 06	1.8900E-01	79	1.2404E 06	3.1540E-01
30	7.1138E 06	1.9360E-01	80	1.1970E 06	3.1230E-01
31	6.8647E 06	1.9810E-01	81	1.1510E 06	3.0750E-01
32	6.6243E 06	2.0270E-01	82	1.1146E 06	3.0220E-01
33	6.3923E 06	2.0740E-01	83	1.0756E 06	2.9640E-01
34	6.1685E 06	2.1210E-01	84	1.0379E 06	2.9030E-01
35	5.9525E 06	2.1640E-01	85	1.0016E 06	2.8380E-01
36	5.7440E 06	2.2040E-01	86	9.6649E 05	2.7700E-01
37	5.5429E 06	2.2420E-01	87	9.3265E 05	2.7000E-01
38	5.3488E 06	2.2790E-01	88	9.0000E 05	2.5180E-01
39	5.1615E 06	2.3150E-01	89	8.3644E 05	2.2080E-01
40	4.9808E 06	2.3490E-01	90	7.7737E 05	1.8670E-01
41	4.8064E 06	2.3840E-01	91	7.2247E 05	1.5040E-01
42	4.6380E 06	2.4180E-01	92	6.7145E 05	1.1260E-01
43	4.4756E 06	2.4520E-01	93	6.2403E 05	7.9640E-02
44	4.3189E 06	2.4840E-01	94	5.7996E 05	5.8360E-02
45	4.1677E 06	2.5190E-01	95	5.3900E 05	3.9970E-02
46	4.0217E 06	2.5530E-01	96	5.0093E 05	2.3900E-02
47	3.8809E 06	2.6220E-01	97	4.6555E 05	9.8650E-03
48	3.7450E 06	2.6220E-01	98	4.3268E 05	5.7930E-04
49	3.6139E 06	2.6560E-01	99	4.0212E 05	0.0
50	3.4873E 06	2.6900E-01	100	3.7373E 05	0.0

Table 1 (Cont'd.)

Group No.	Upper Energy (eV)	Detector Efficiency
101	3.4733E 05	0.0
102	3.2280E 05	0.0
103	3.0000E 05	0.0
104	1.0000E 07	1.7190E-01
105	9.5000E 06	1.6610E-01
106	9.0000E 06	1.5980E-01
107	8.5000E 06	1.5400E-01
108	8.0000E 06	1.4790E-01
109	7.5000E 06	1.4340E-01
110	7.2000E 06	1.3910E-01
111	6.8000E 06	1.3490E-01
112	6.5000E 06	1.3180E-01
113	6.2000E 06	1.2870E-01
114	6.0000E 06	1.2740E-01
115	5.8000E 06	1.2660E-01
116	5.6000E 06	1.2580E-01
117	5.4000E 06	1.2480E-01
118	5.2000E 06	1.2390E-01
119	5.0000E 06	1.2270E-01
120	4.8000E 06	1.2160E-01
121	4.6000E 06	1.2000E-01
122	4.2000E 06	1.1860E-01
123	4.0000E 06	1.1770E-01
124	3.8000E 06	1.1680E-01
125	3.6000E 06	1.1580E-01
126	3.4000E 06	1.1470E-01
127	3.2000E 06	1.1340E-01
128	3.0000E 06	1.1210E-01
129	2.8000E 06	1.1080E-01
130	2.6000E 06	1.1000E-01
131	2.4000E 06	1.0890E-01
132	2.2000E 06	1.0690E-01
133	2.0000E 06	1.0400E-01
134	1.8000E 06	1.0120E-01
135	1.6000E 06	9.6200E-02
136	1.4000E 06	8.8400E-02
137	1.2000E 06	7.4600E-02
138	1.0000E 06	4.2600E-02
139	8.0000E 05	2.6000E-03
140	6.0000E 05	0.0
141	4.0000E 05	0.0

$$\Delta t = (R1 - R2) \times T \qquad (1)$$

where R1 and R2 are random numbers and T = 12 nsec.

The calculation model for the ORNL experiment is shown in Fig. 3. Neither the fill tube nor the styrofoam dewar support structure were included in mocking up the Pyrex dewar. The detector coordinates include the 2-deg rotation between the beam and detector axis in the experiment.

Count rates were calculated as $\phi \times \varepsilon$ where ϕ is the flux at the detector center determined by next flight estimation and ε is the detector efficiency given in Table 1. The count rates were converted to counts per MeV per incident source neutron by multiplying the count rate by the time bin width and by dividing by the corresponding energy group width in MeV. The fraction of incident neutrons in each energy group is equal (within statistics) since the group boundaries are equally spaced in lethargy and the starting energies were selected uniformly in lethargy.

The detector count rates were reported as functions of the incident neutron energy. The time bins for the calculation were determined from the energy group boundaries, E, as follows:

$$T = \frac{D/C}{\sqrt{1 - \frac{1}{\left(1 + \frac{E'}{2c^2}\right)^2}}} \qquad (2)$$

where,

T = flight time in sec from accelerator source to sample face for a neutron energy E at the source,

D = distance in cm from accelerator source to sample face,

$E' = 1.06434 \times 10^{-3} \times E$, where E is the energy in MeV,

c = speed of light in cm/sec.

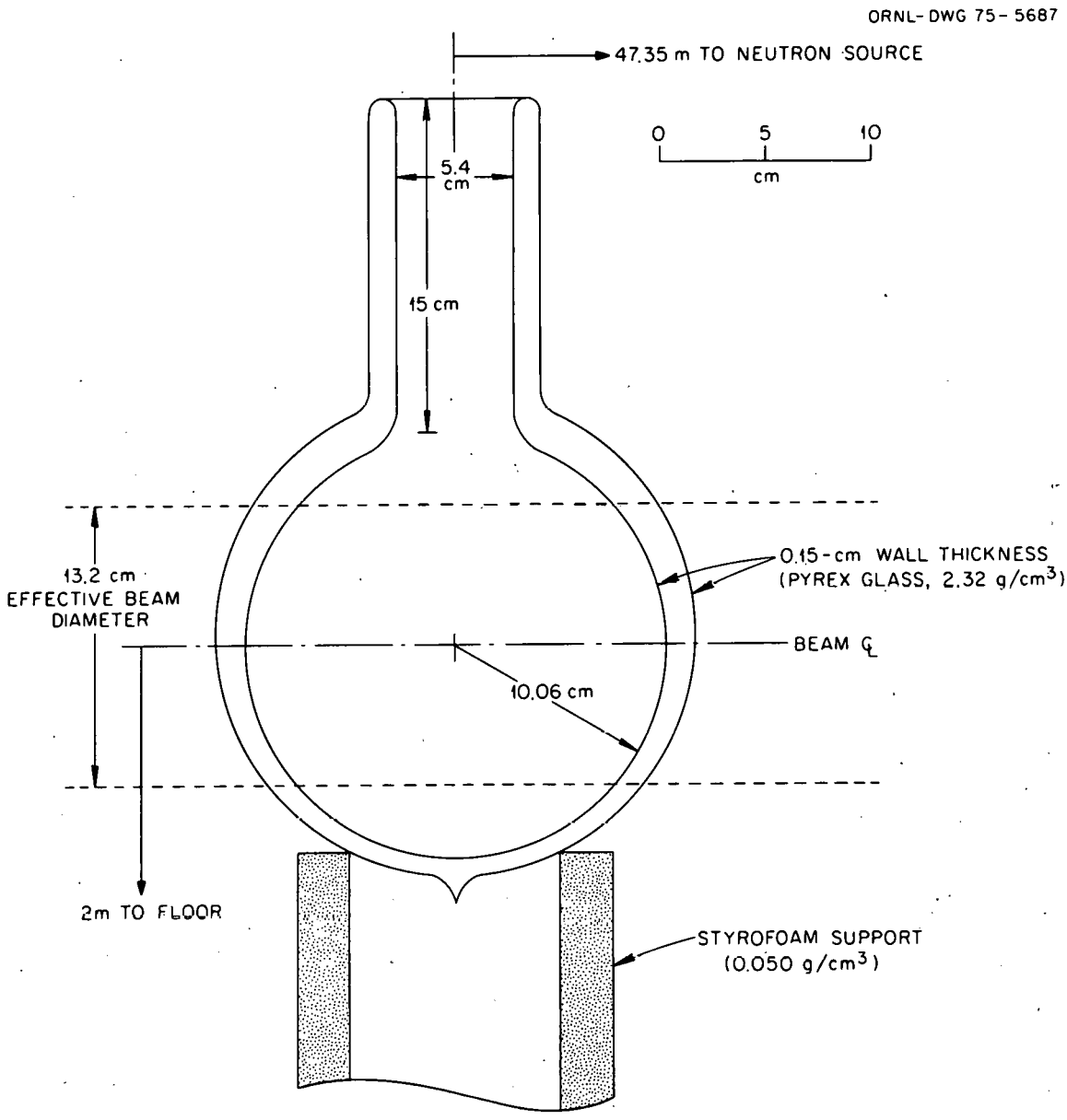

Fig. 3. Geometry of Oxygen Dewar Used in ORNL Experiment.

Although the neutron flight times scattering in the sample and travelling to the detector are included in the calculations, they are generally small compared to the flight time of the neutrons from the source to the sample as determined by Eq. (2).

The calculated secondary energy spectra for the experiment included the empirically determined energy resolution of the detector given by R, the full-width at half-maximum of the resolution function in percent:

$$R = \sqrt{A + B/E} \tag{3}$$

where A was 250 for neutrons and 170 for gamma rays, B was 670 for neutrons and 288 for gamma rays, and E was an energy in MeV uniformly selected in the energy group of the detected particle. The spectra were obtained by time-dependent calculations with time bins being determined by Eq. (2) where E corresponded to the broad group energy boundaries used in unfolding the experimental pulse-height spectra.

IV. Comparison of Experimental and Calculated Results

The figures which follow summarize the calculations performed for comparison with the experimental data. All calculations were made with the MORSE Monte Carlo code using the ENDF/B-IV oxygen cross-section set. The integral count rate comparisons for both neutrons and gamma rays at the various detector locations are given in Figs. 4 to 7. In all figures the error bars represent one standard deviation of the mean value. Figures 8 through 31 give the secondary energy spectra comparisons for both neutrons and gamma rays at all four detector angles. In the multiple energy spectra figures, each set of comparisons is plotted at the mid-point of the appropriate incident neutron energy bin (i.e., the plot at 11.25 MeV on the slanted energy scale corresponds to the spectrum of secondary neutrons arising from incident neutrons in the 10.0 to 12.5 MeV energy range).

V. Discussion

The integral neutron count rate comparisons in Figs. 4 through 7 are generally in good agreement except for the 10% to 40% disagreements in the neutron results above 10 MeV at all angles, and at 3 MeV and above 4 MeV at 30 deg. In these latter comparisons the calculations are uniformly higher than the experimental results. The gamma-ray integral result comparisons show excellent agreement at all angles and energies above the 6 MeV threshold for inelastic gamma-ray production in oxygen. Results below this energy have large statistical errors and are the result of gamma-ray production in the glass dewar and other background sources.

Looking closely at the unfolded neutron spectra comparisons for the 30-deg detector it is clear that the major reason for the discrepancies in the 30-deg integral results is the disagreement between the measurements and the calculations for elastic scattering. The calculated detector response for the high energy side of the peak resulting from elastic scattering in the oxygen sample is uniformly high for all of the incident neutron energy bins shown in Figs. 8, 9, and 10. This disagreement is most pronounced in the 2-3 MeV energy bin where the calculated kinematics of elastic scattering appear to indicate that most of the events in this bin come from incident neutrons with energies above the 2.3 MeV oxygen total cross section minimum. The experimental results show the opposite in that most scatterings occur below the 2.3 MeV minimum. Since the high energy side of the elastic peak in each energy bin is most sensitive to small angle scattering (less than 30 deg) from the region of the dewar being hit by the beam, it appears likely that the P_7 Legendre representation of the low angle scattering is not sufficient for such a high resolution angular measurement. Similar results were found for nitrogen integral measurements,[1] so it seems unlikely that it is the oxygen data that is at fault. Small angle scattering cross-section measurements in both nitrogen and oxygen are not available to verify this conclusion, however, and runs using higher order P_ℓ expansions would be prohibitively expensive and limited by core storage requirements.

A discrepancy not evident in the integral results which does appear in the spectral comparisons is the discrepancy in the first level inelastic scattering peak for oxygen (shown about 6 MeV below the elastic peak in each energy bin of the spectra figures) at incident neutron energies above the inelastic threshold of 6 MeV. The calculations of inelastic scattering at almost all angles (see Figs. 8 to 19) appear to be low with the effect most pronounced at incident energies right above threshold. This strongly indicates that the first level inelastic cross section at these energies is low by from 10%-20%. Further evidence for this conclusion can be inferred from the secondary gamma-ray spectra where the calculated gamma-ray production from the 6 MeV first inelastic level (producing a 6 MeV gamma ray) is uniformly low for incident neutron energies greater than 6 MeV (see Figs. 20 to 31). A similar but smaller discrepancy occurs in the inelastic scattering from the cluster of discrete levels in oxygen from 12-13 MeV where the calculations appear to be high (see Figs. 13 and 16).

The spectral comparisons for gamma-ray production appear to show substantial discrepancies not apparent from the integral results shown in Figs. 4 to 7. The only important discrepancy, however, is the one discussed above in connection with underpredicting gamma-ray production from first level inelastic scattering events in oxygen. The large discrepancies in the results for neutron energies below the 6 MeV oxygen threshold indicate that the gamma-ray background (possibly from the boron in the glass dewar) was not calculated properly.

VI. Conclusions

The current ENDF/B-IV neutron and gamma-ray production data for oxygen above 1 MeV appear to be in good order based on the comparisons of calculated and measured integral and differential results made in this study. The only major discrepancy uncovered was related to neutron scattering and gamma-ray production from first level inelastic scattering interactions. Calculated results for the production of 6 MeV gamma rays from the 6 MeV first inelastic level in oxygen appear to be low by

around 50% at energies above the inelastic threshold. Likewise, calculated secondary neutron spectra for incident neutron energies above 6 MeV are uniformly low at energies corresponding to neutrons having had first level inelastic scattering events in oxygen.

Additional deficiencies in the oxygen cross-section data are indicated for inelastic scattering from the cluster of discrete levels in the 12-13 MeV range and for elastic scattering at very small angles at energies above 2 MeV. In both cases the data give rise to overprediction of the calculated results of these events. In the case of forward scattering, however, calculational model deficiencies are the more likely explanation of the discrepancies that were found.

It should be noted that the size of the inelastic discrepancies are larger than the 20-30% order of error indicated for these cross sections in the ENDF/B-IV uncertainty files for oxygen.[8] The effect of such discrepancies on the results of an earlier air transport study[9] are minimal mainly because of the low importance of oxygen data in general other than the 2.3 MeV total cross section minimum. The effects probably do become more important in concrete shielded structures but no quantitative measure of the effect can be quoted as yet.[10]

Acknowledgements

The authors wish to acknowledge the aid of J. D. Drischler in preparing the plotted results. The multigroup cross sections were generated by W. E. Ford, III, of the Computer Science Division.

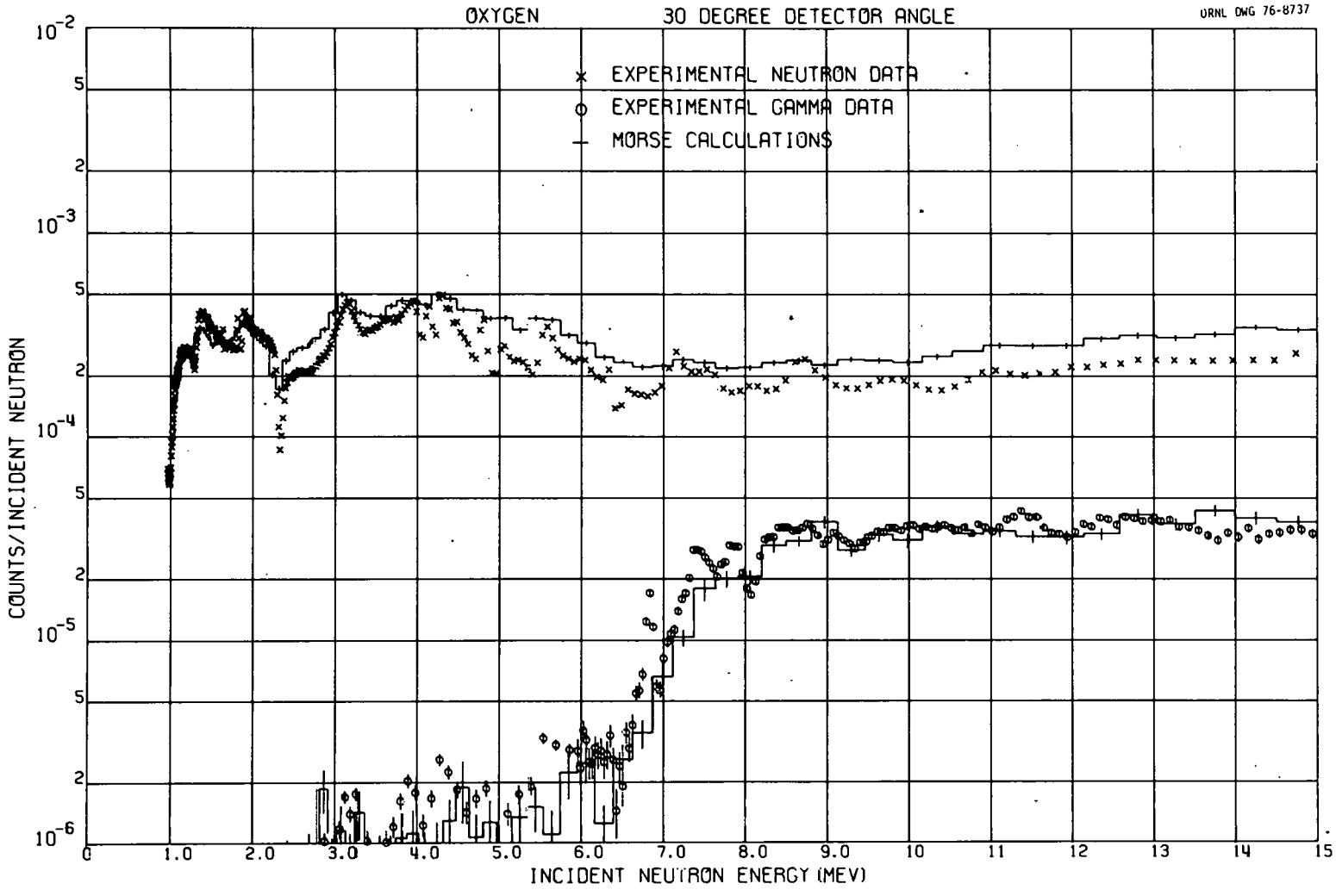

Fig 4. Comparison of Neutron and Gamma-Ray Integral Results at 30 deg with Calculations Using ENDF/B-IV Oxygen Data.

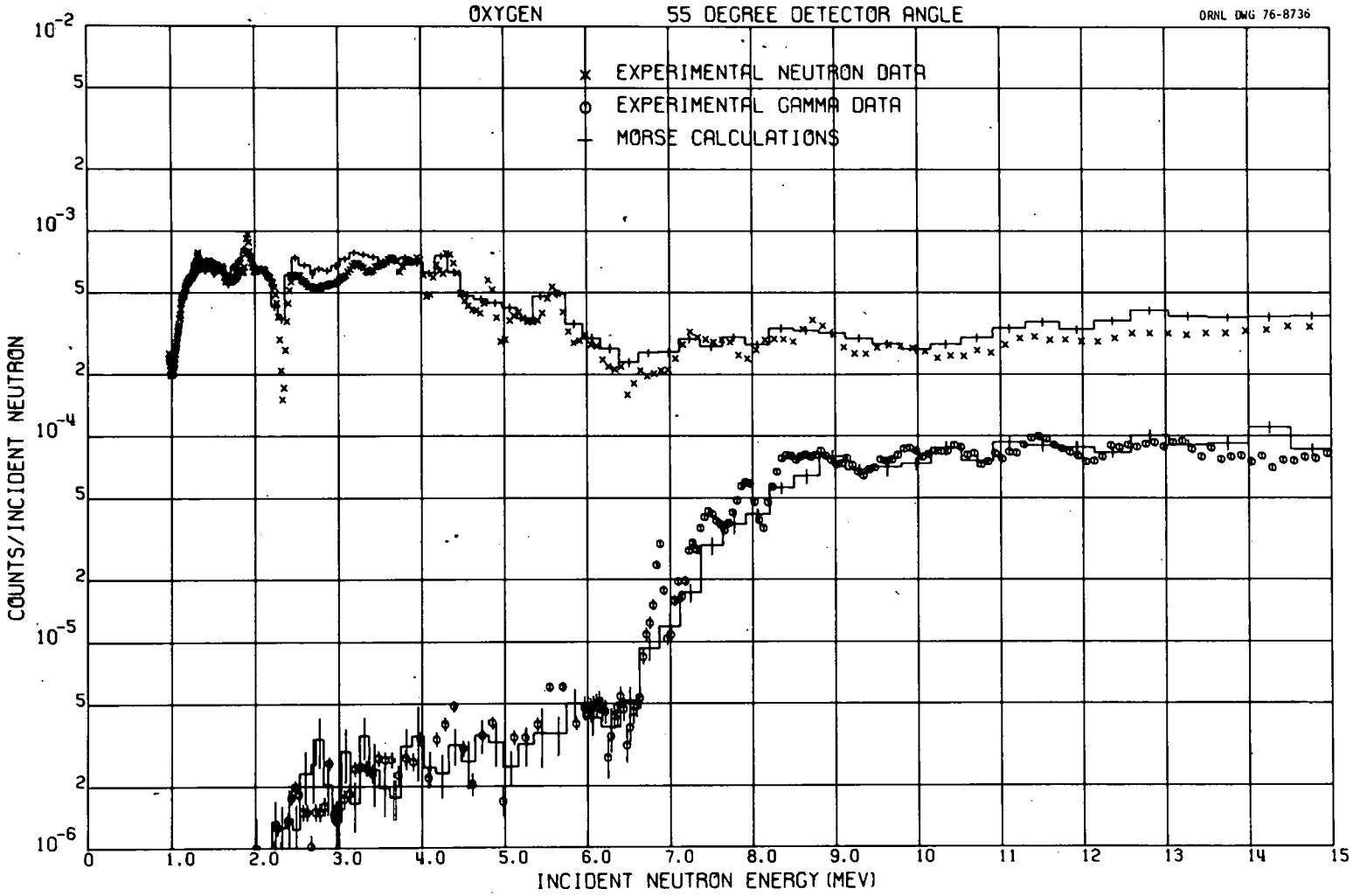

Fig. 5. Comparison of Neutron and Gamma-Ray Integral Results at 55 deg with Calculations Using ENDF/B-IV Oxygen Data.

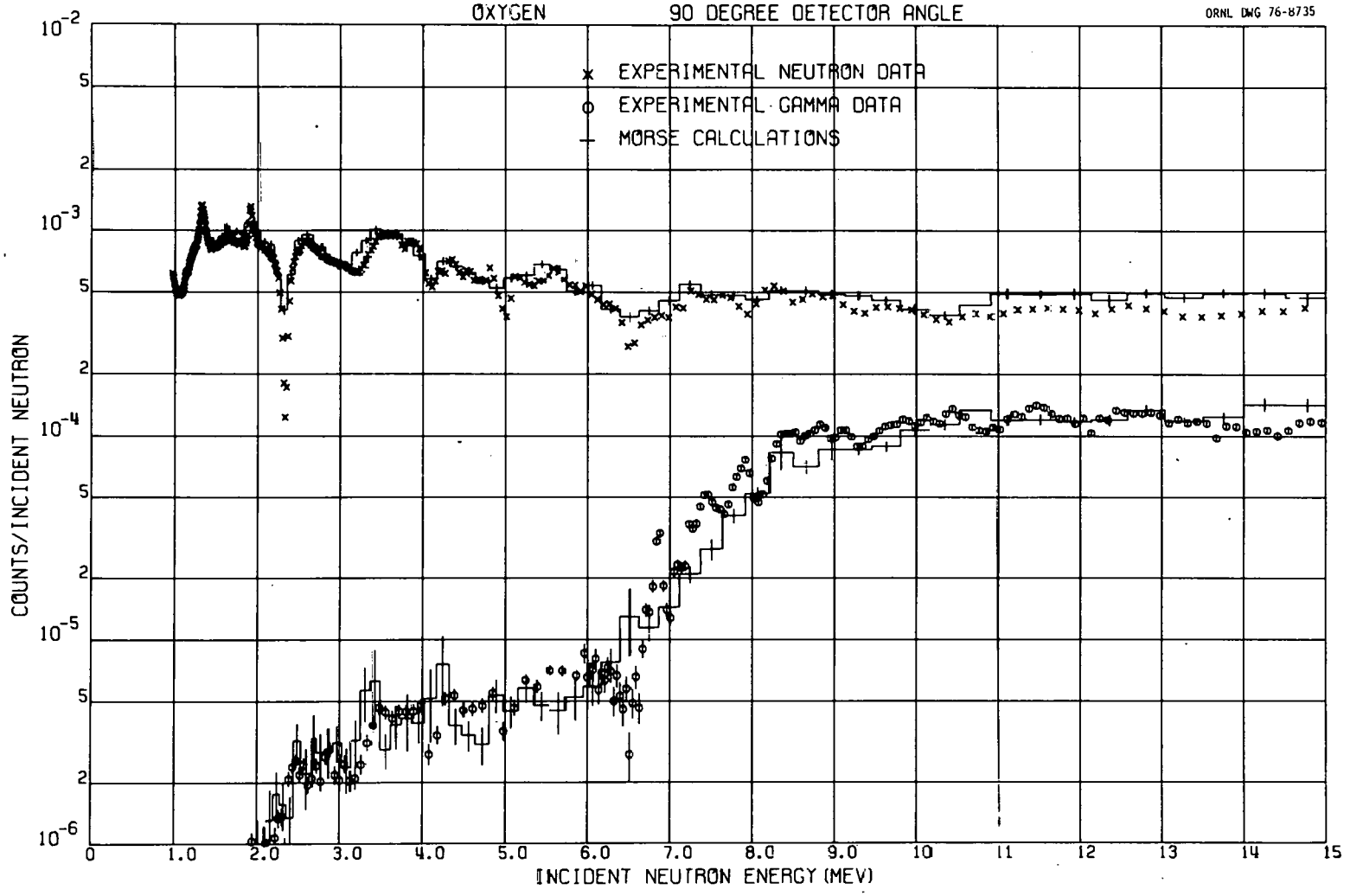

Fig. 6. Comparison of Neutron and Gamma-Ray Integral Results at 90 deg with Calculations Using ENDF/B-IV Oxygen Data.

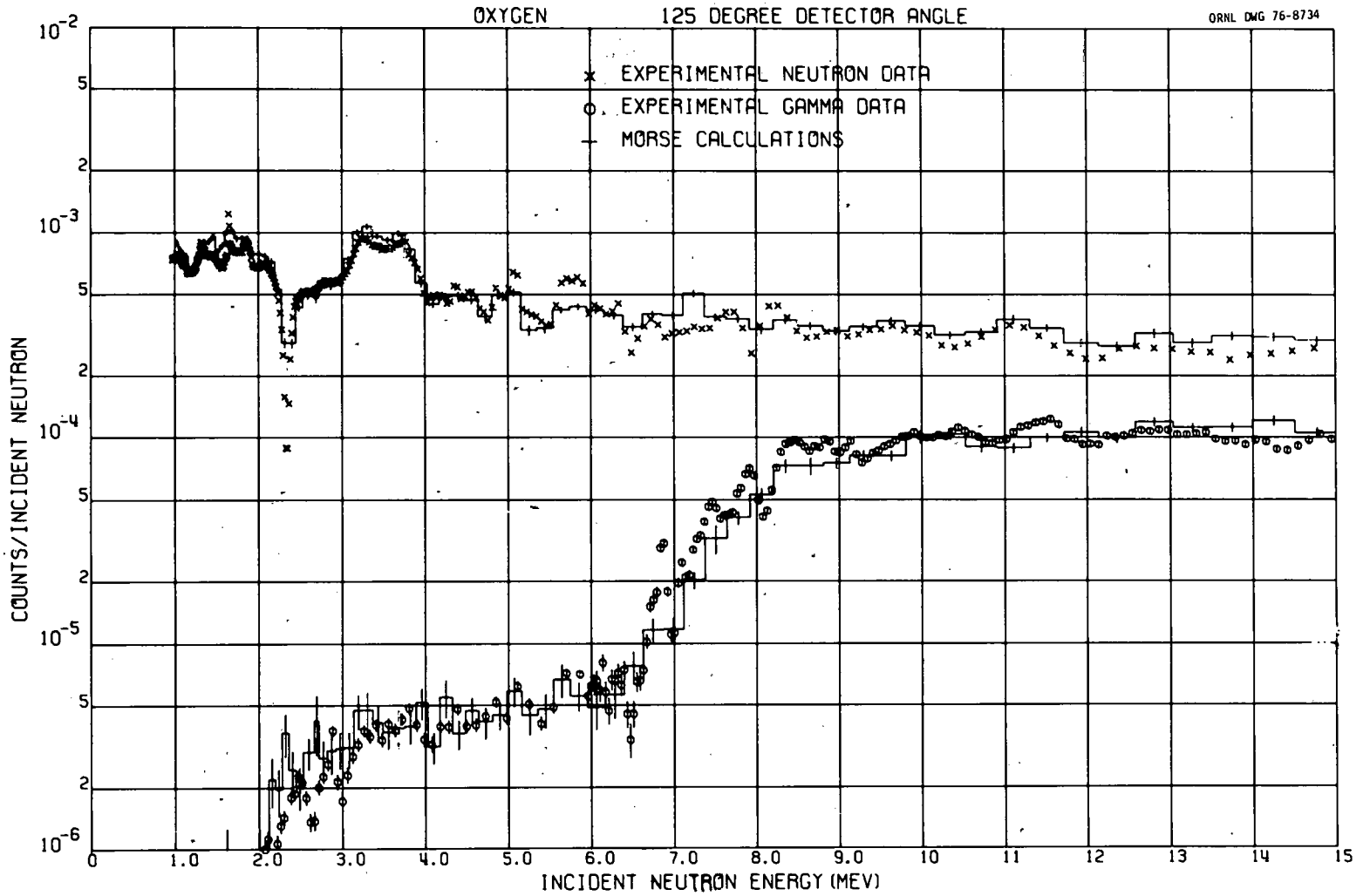

Fig. 7. Comparison of Neutron and Gamma-Ray Integral Results at 125 deg with Calculations Using ENDF/B-IV Oxygen Data.

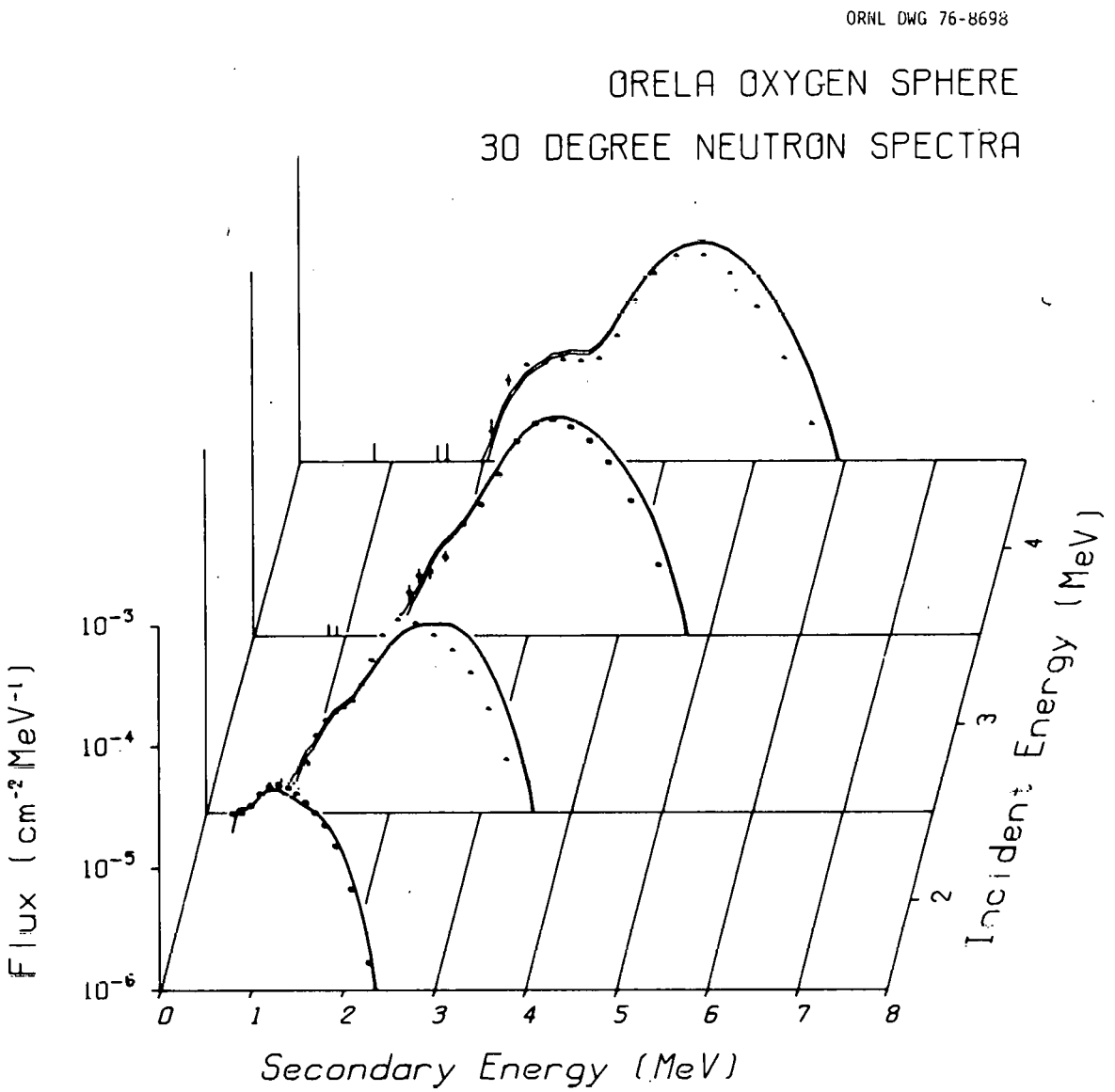

Fig. 8. Secondary Neutron Spectra Comparisons at 30 deg Using ENDF/B-IV Oxygen Data.

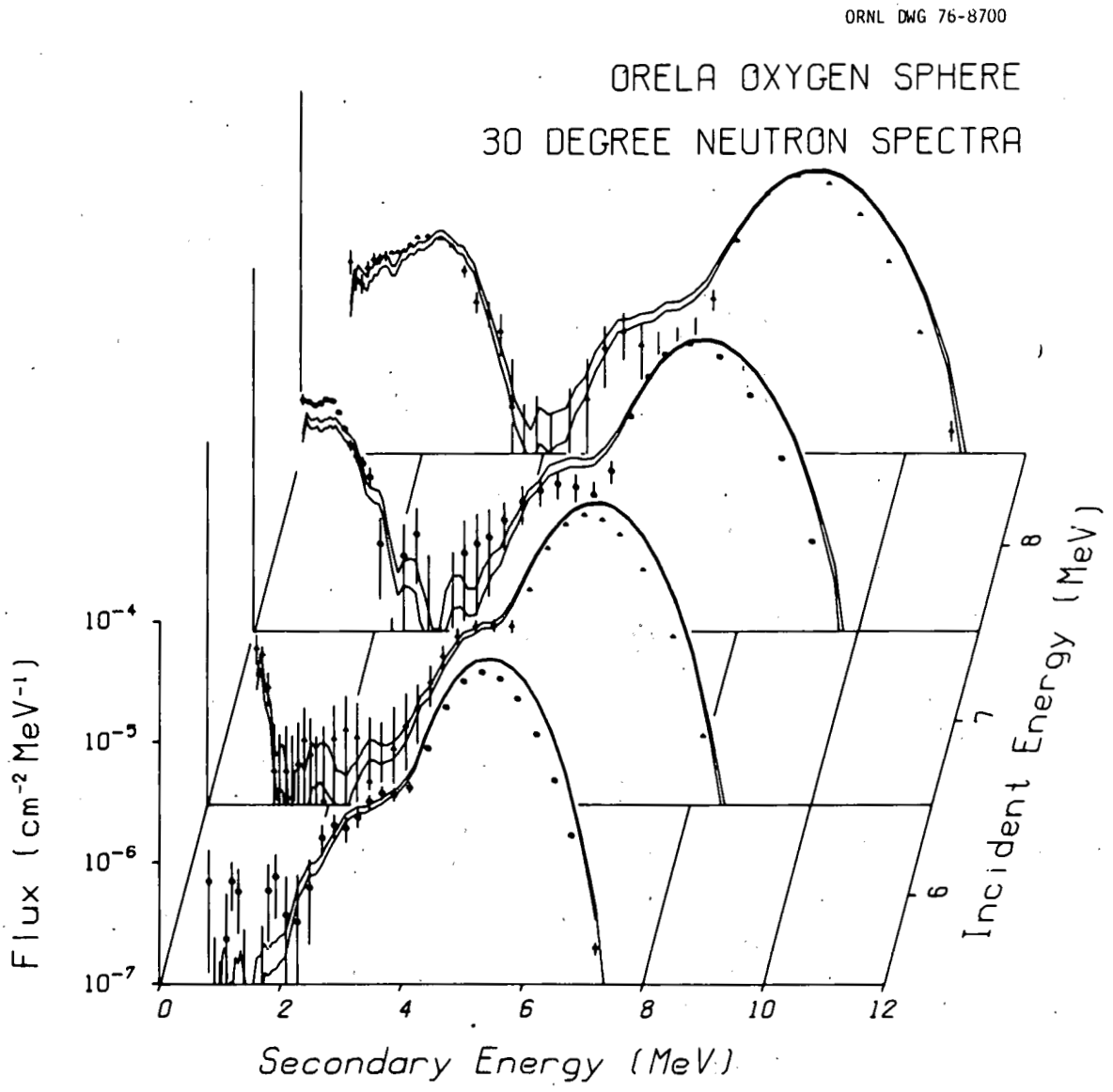

Fig. 9. Secondary Neutron Spectra Comparisons at 30 deg Using ENDF/B-IV Oxygen Data.

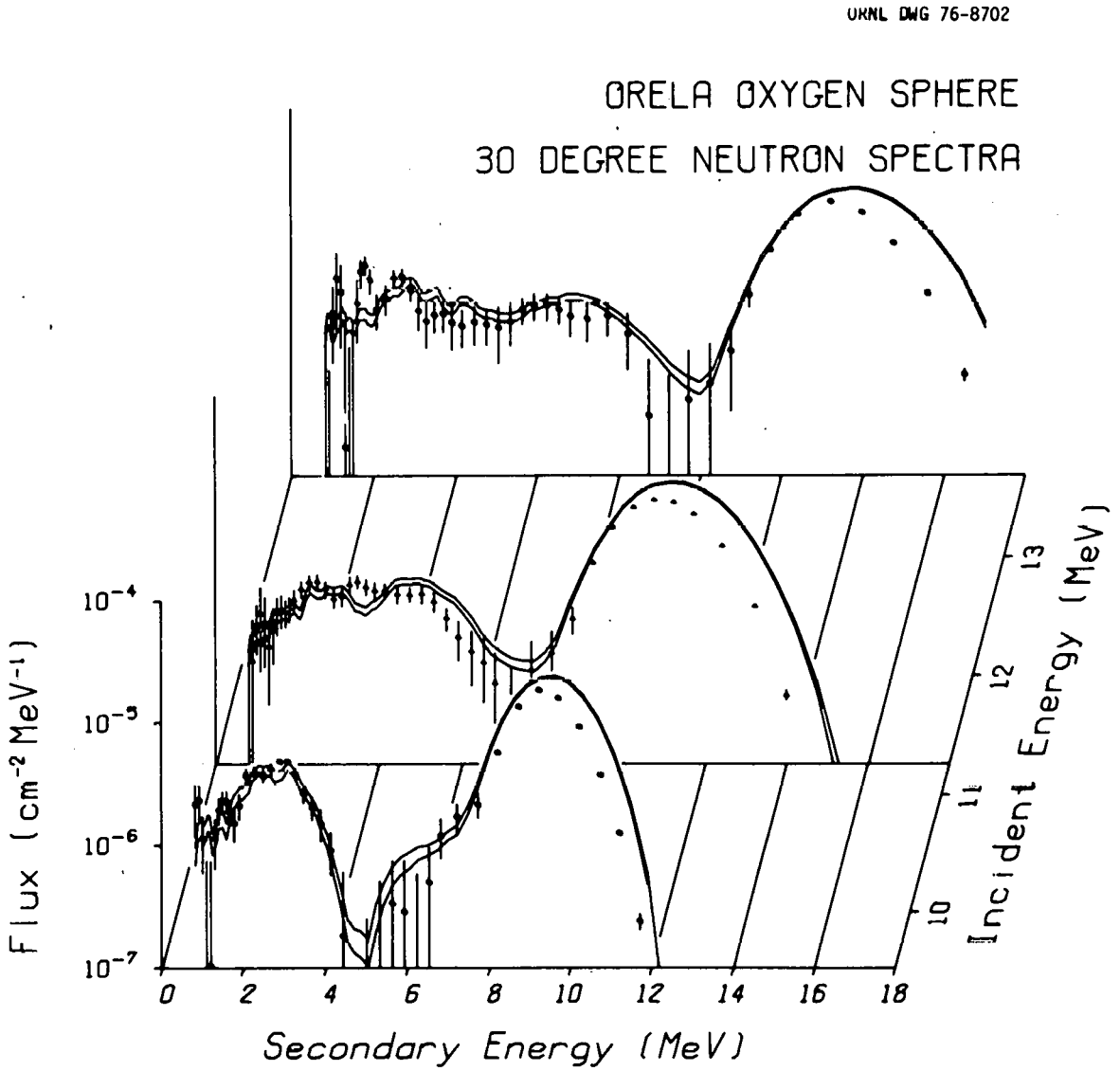

Fig. 10. Secondary Neutron Spectra Comparisons at 30 deg Using ENDF/B-IV Oxygen Data.

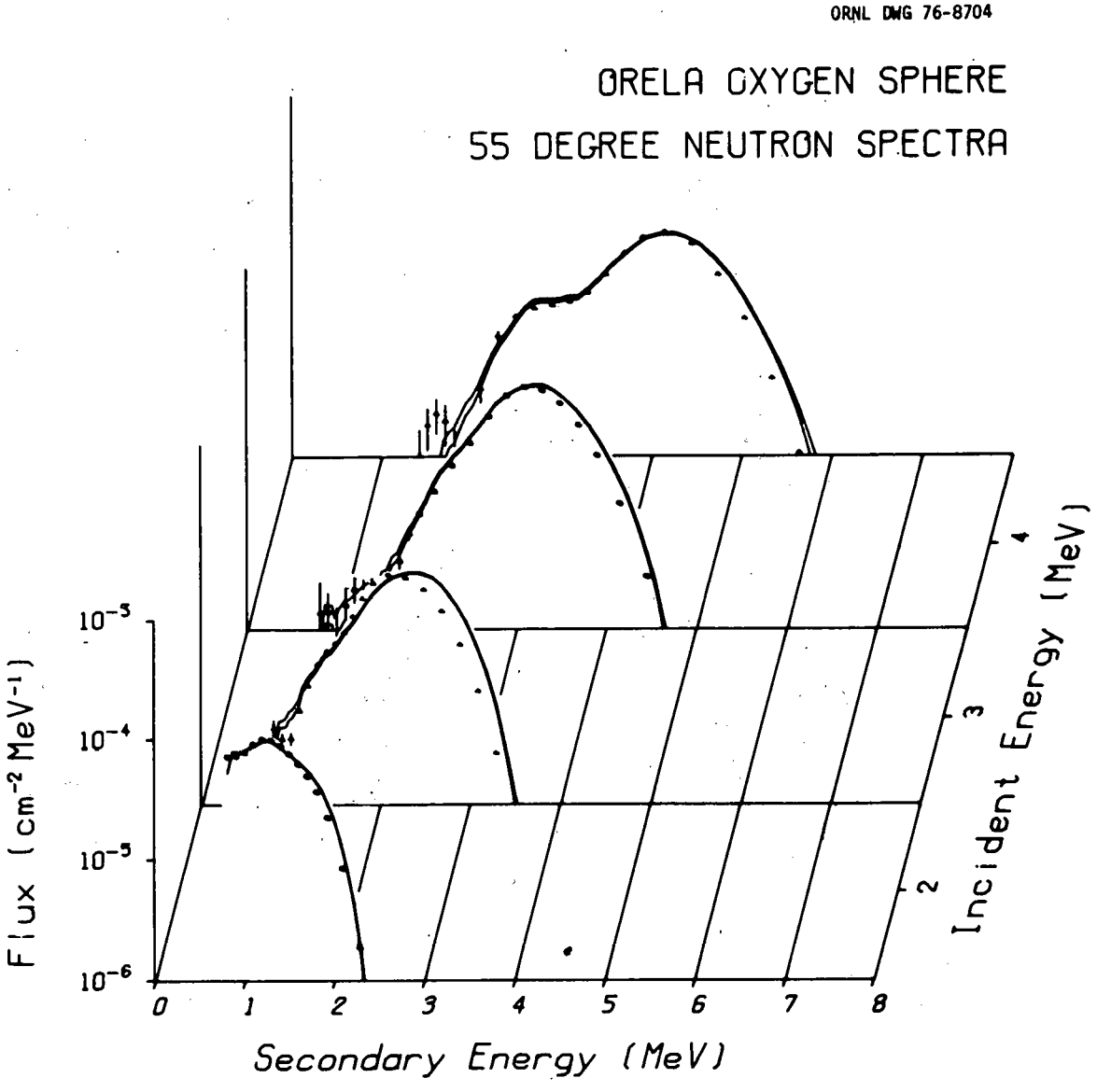

Fig. 11. Secondary Neutron Spectra Comparisons at 55 deg Using ENDF/B-IV Oxygen Data.

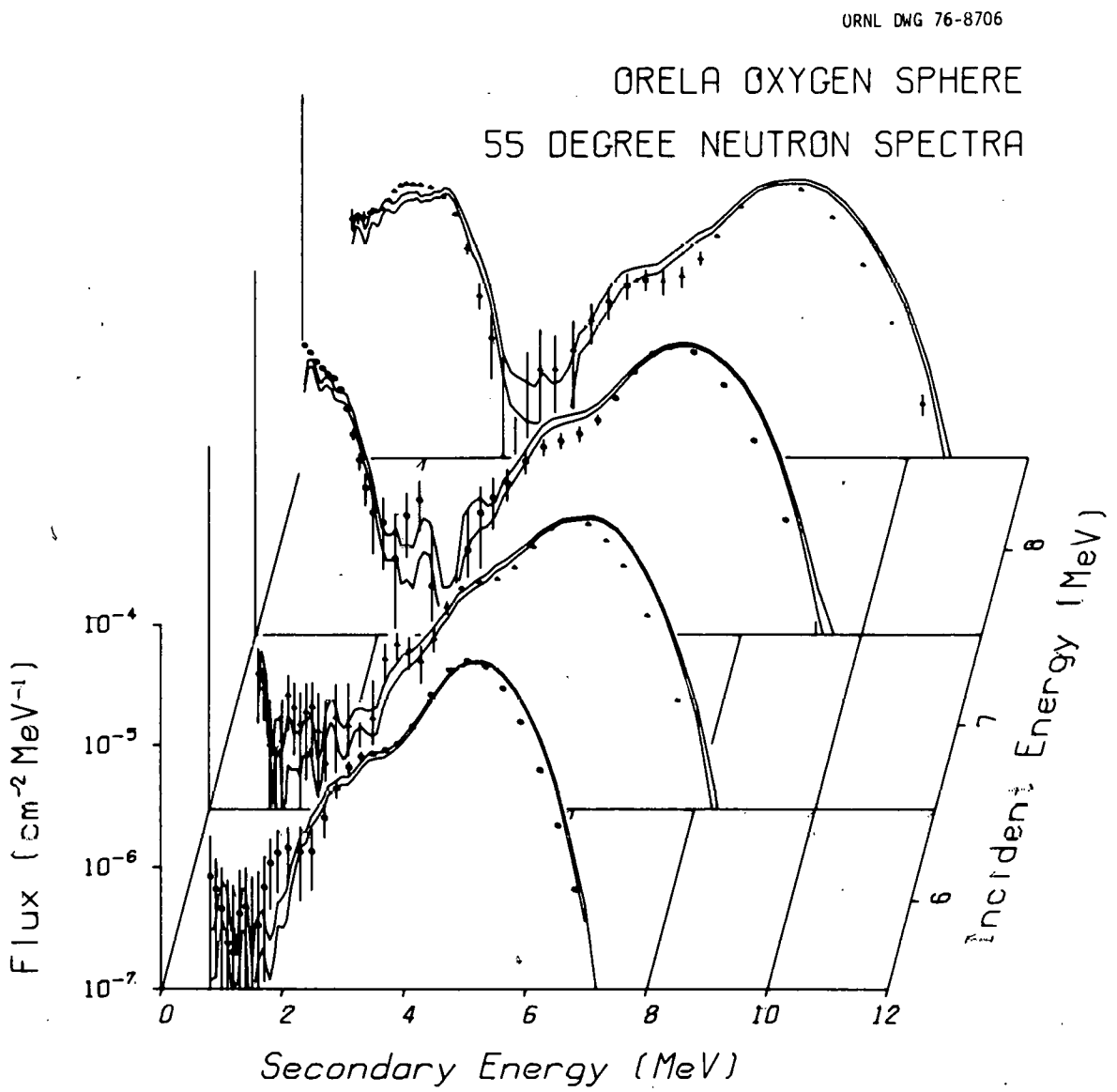

Fig. 12. Secondary Neutron Spectra Comparisons at 55 deg Using ENDF/B-IV Oxygen Data.

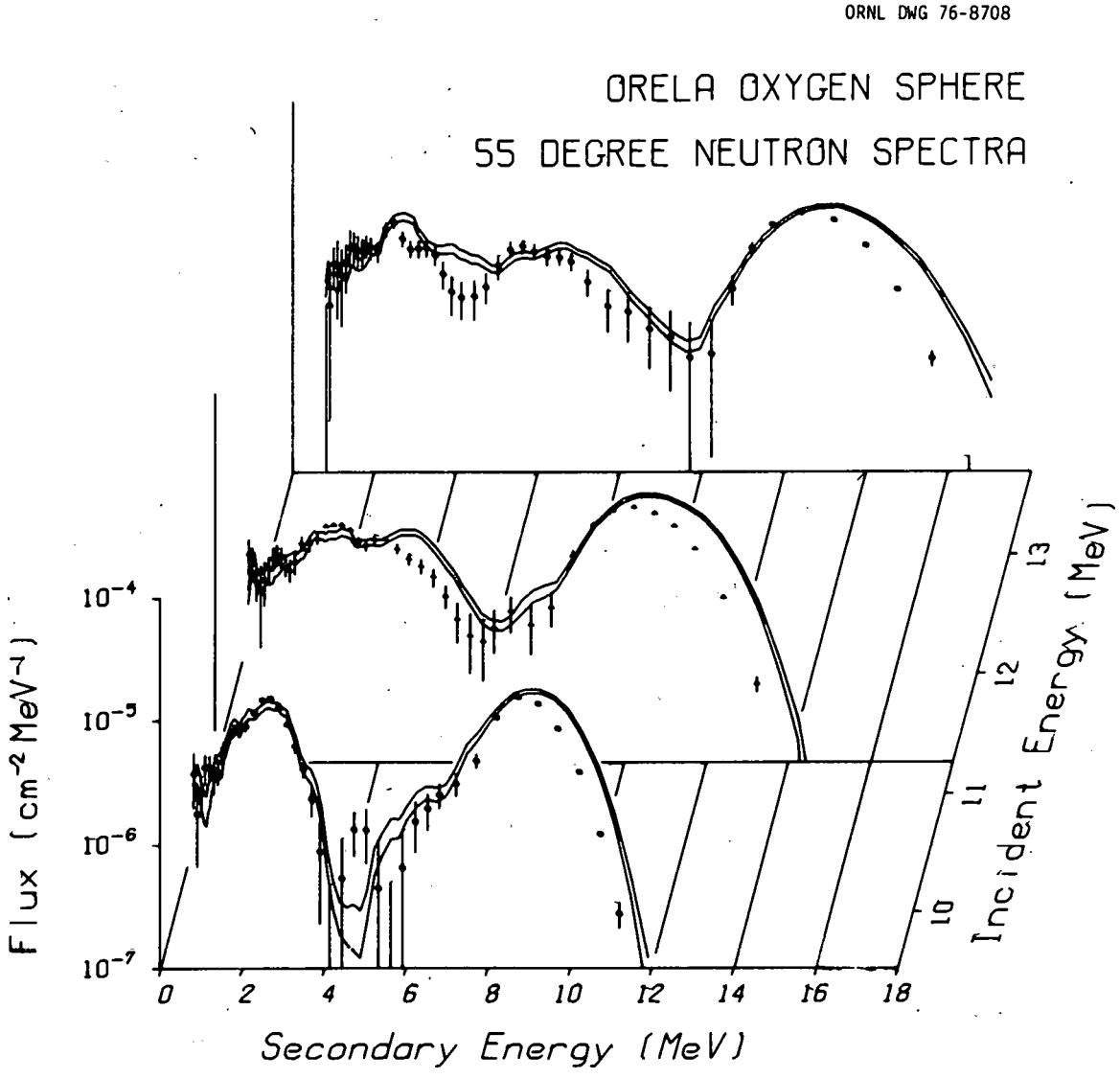

Fig. 13. Secondary Neutron Spectra Comparisons at 55 deg Using ENDF/B-IV Oxygen Data.

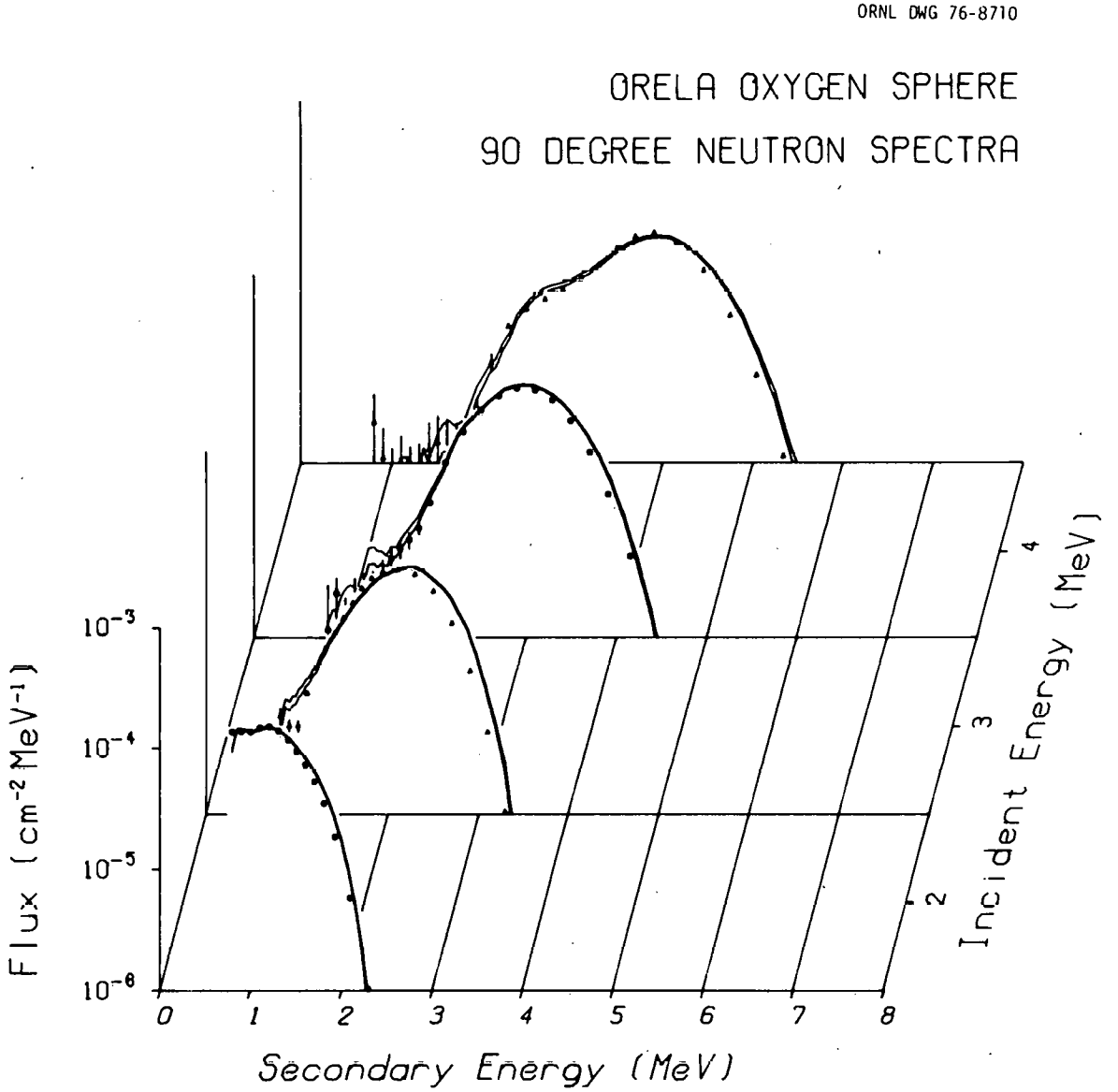

Fig. 14. Secondary Neutron Spectra Comparisons at 90 deg Using ENDF/B-IV Oxygen Data.

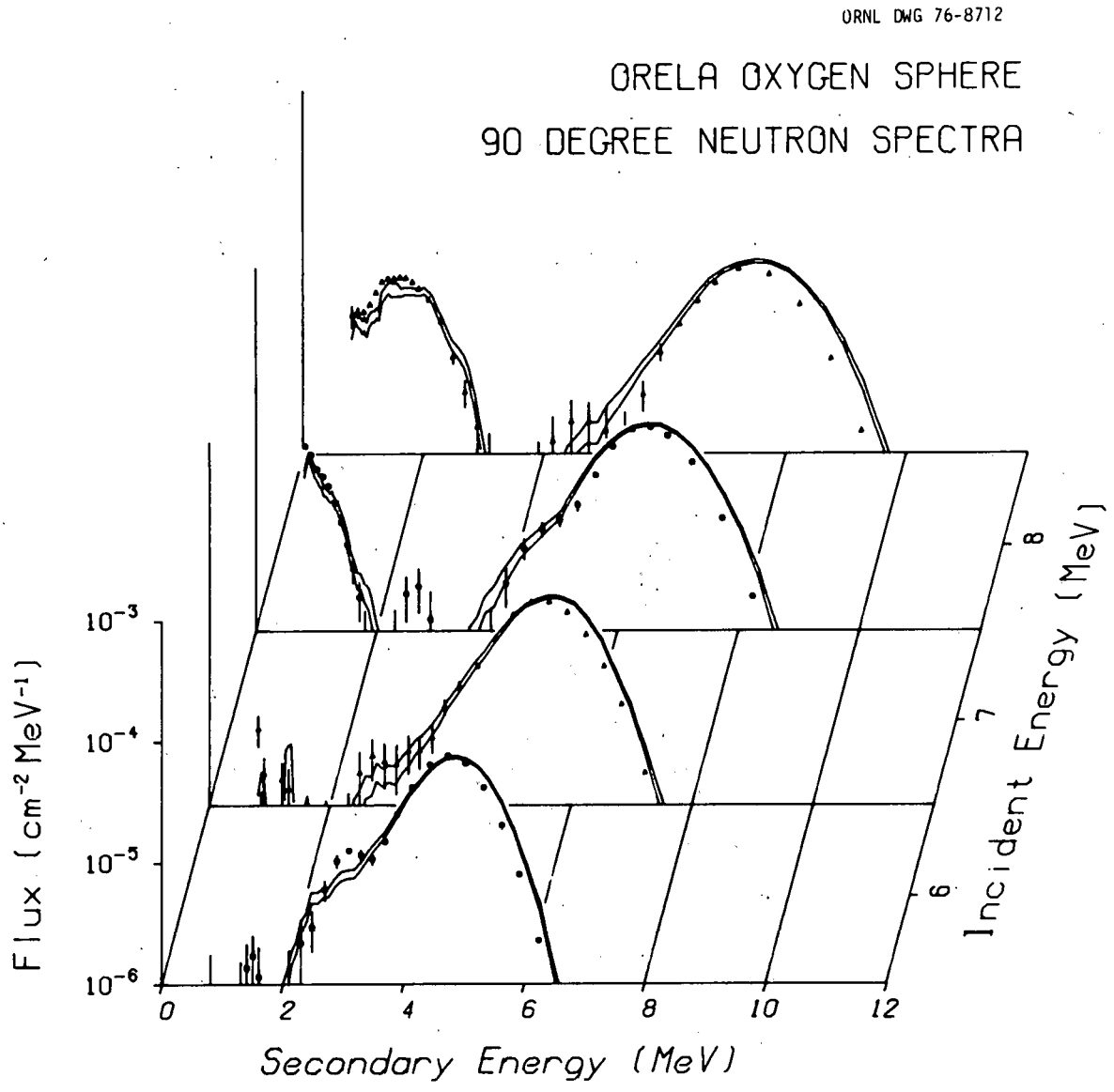

Fig. 15. Secondary Neutron Spectra Comparisons at 90 deg Using ENDF/B-IV Oxygen Data.

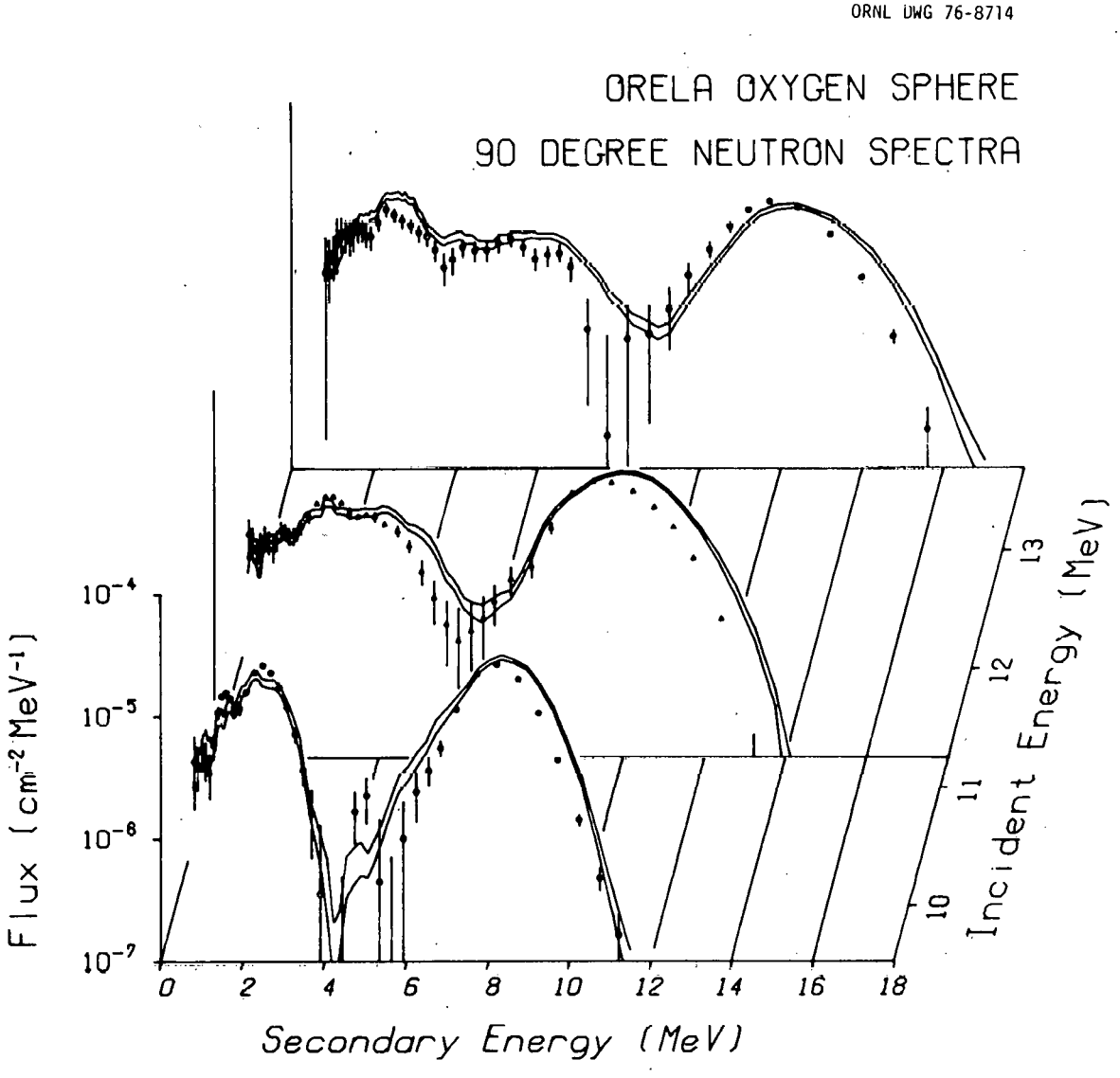

Fig. 16. Secondary Neutron Spectra Comparisons at 90 deg Using ENDF/B-IV Oxygen Data.

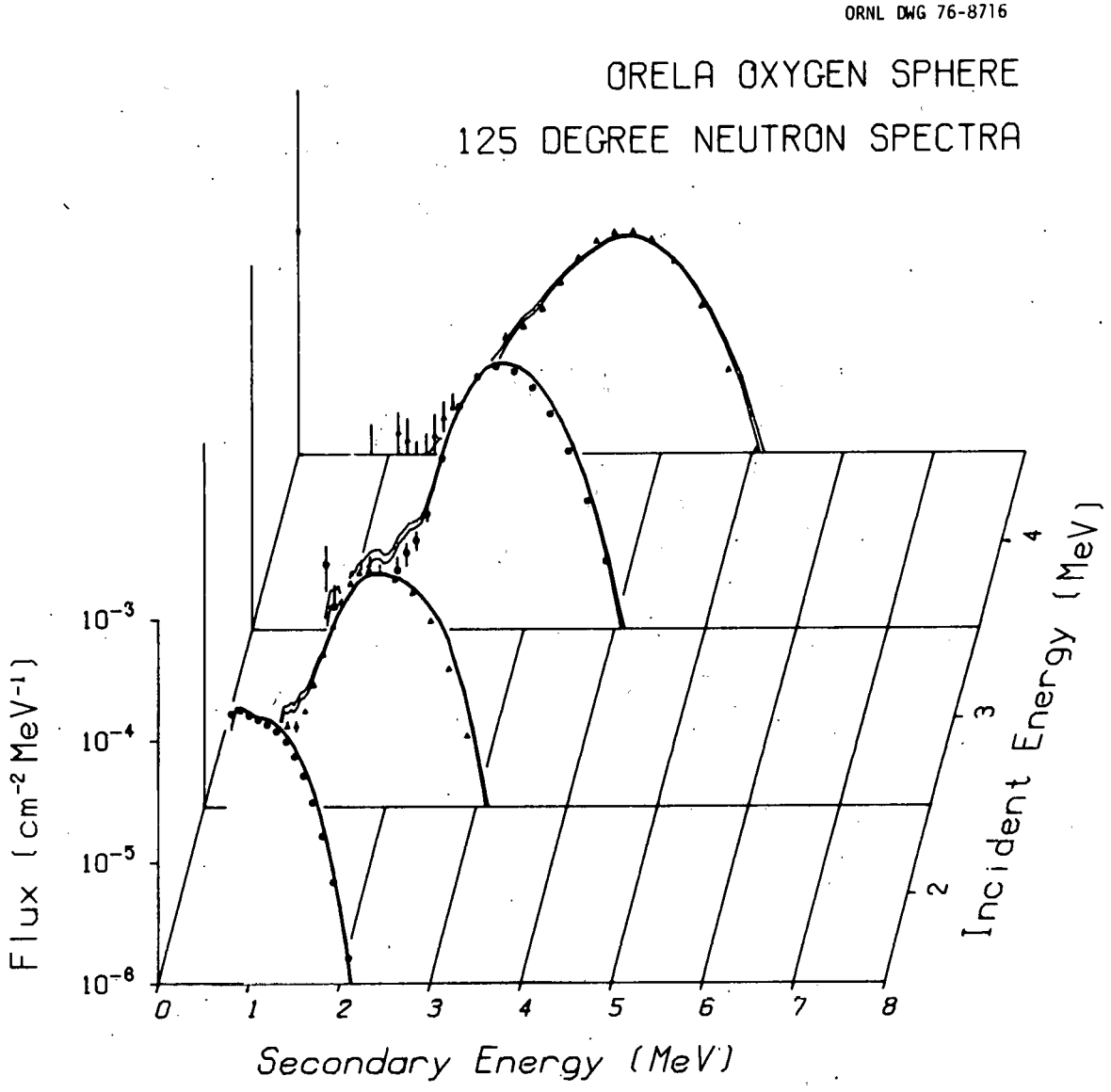

Fig. 17. Secondary Neutron Spectra Comparisons at 125 deg Using ENDF/B-IV Oxygen Data.

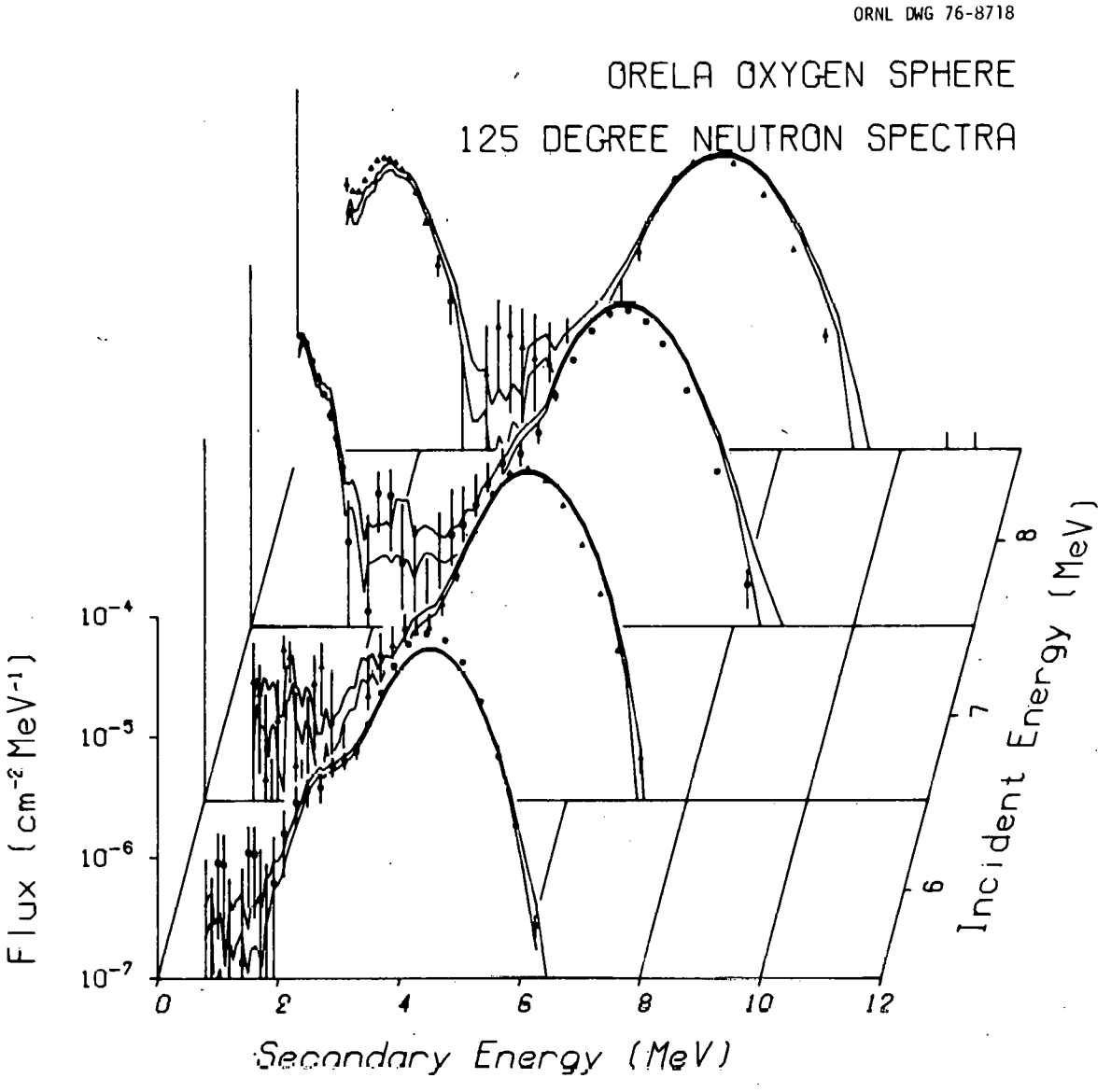

Fig. 18. Secondary Neutron Spectra Comparisons at 125 deg Using ENDF/B-IV Oxygen Data.

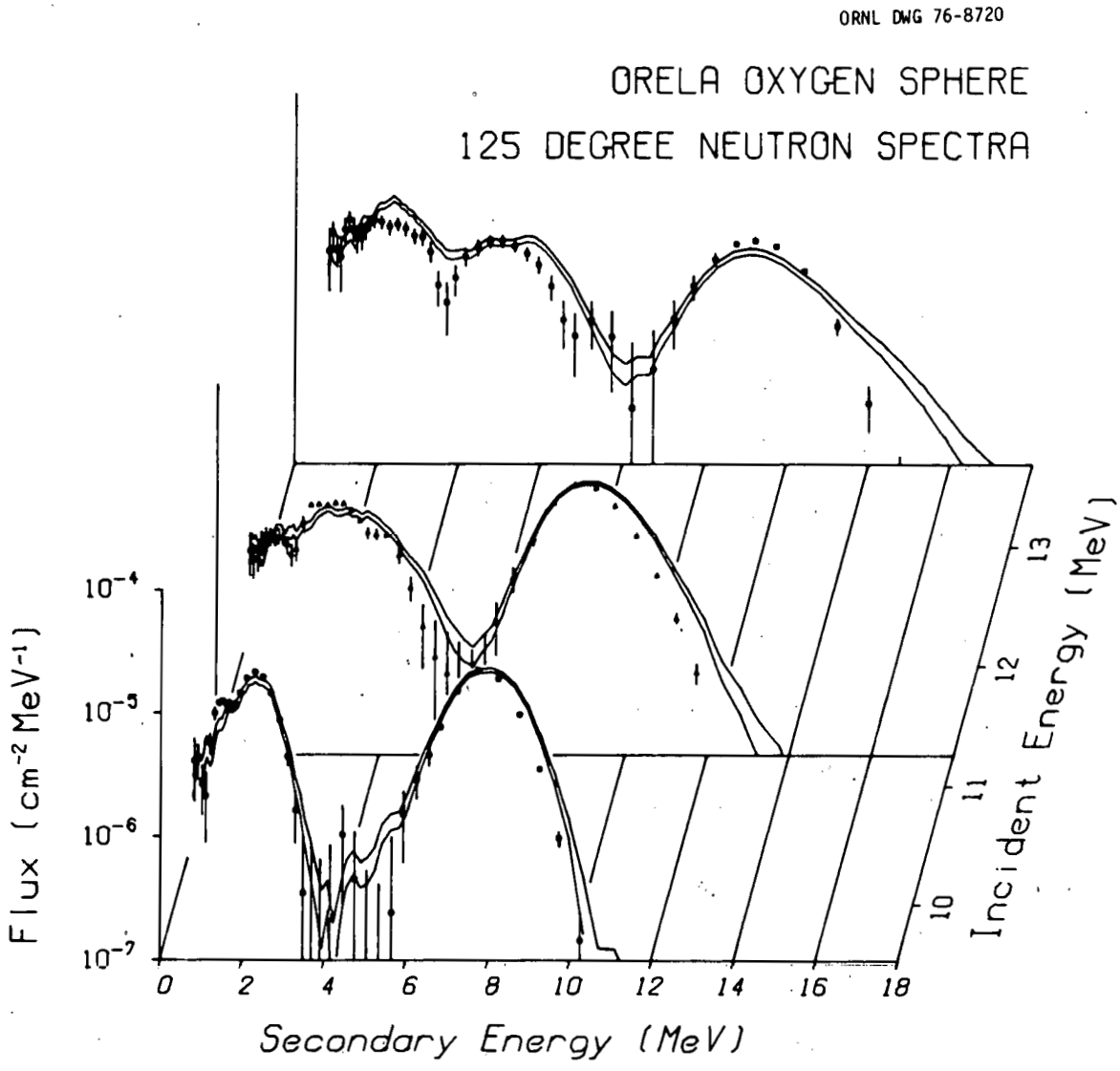

Fig. 19. Secondary Neutron Spectra Comparisons at 125 deg Using ENDF/B-IV Oxygen Data.

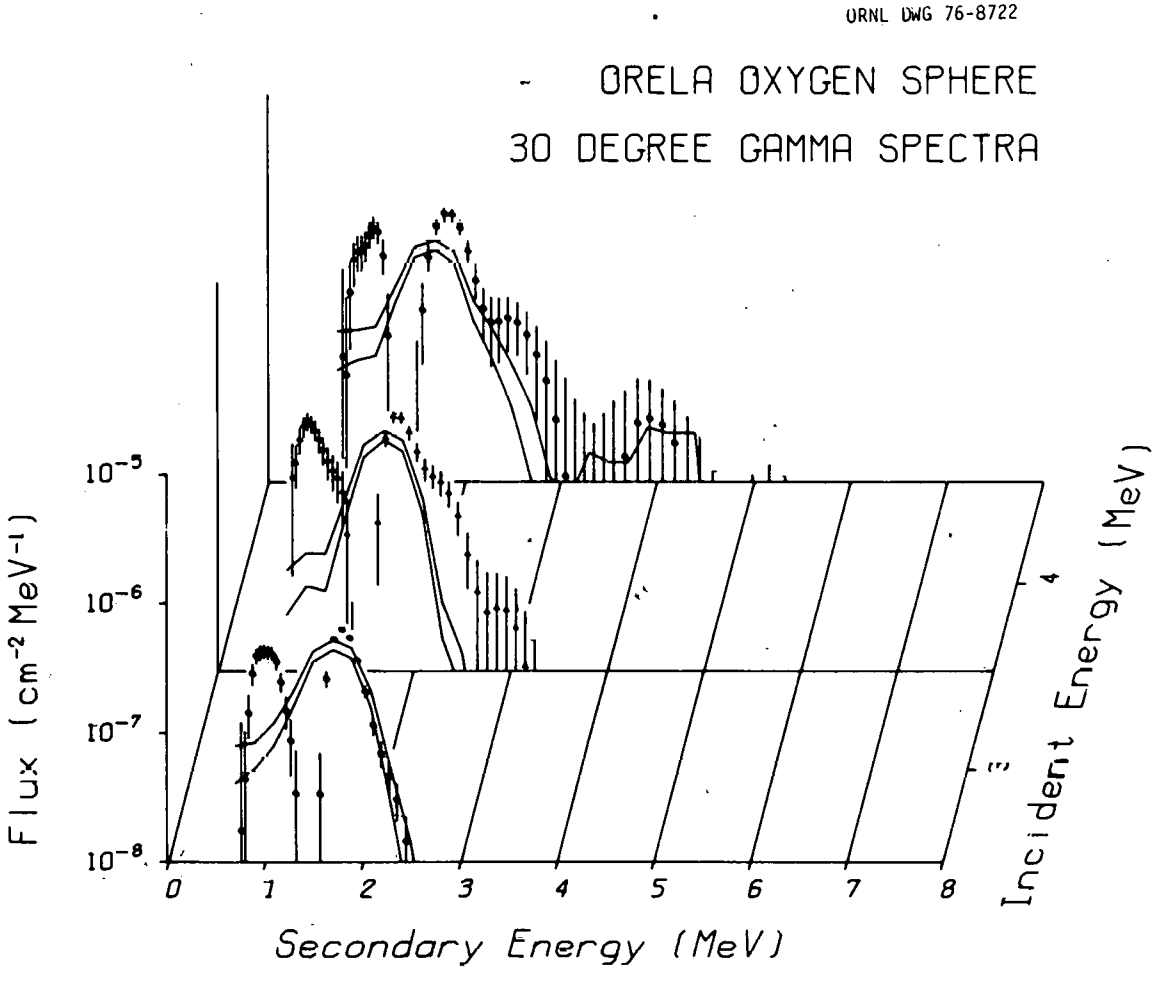

Fig. 20. Secondary Gamma-Ray Spectra Comparisons at 30 deg Using ENDF/B-IV Oxygen Data.

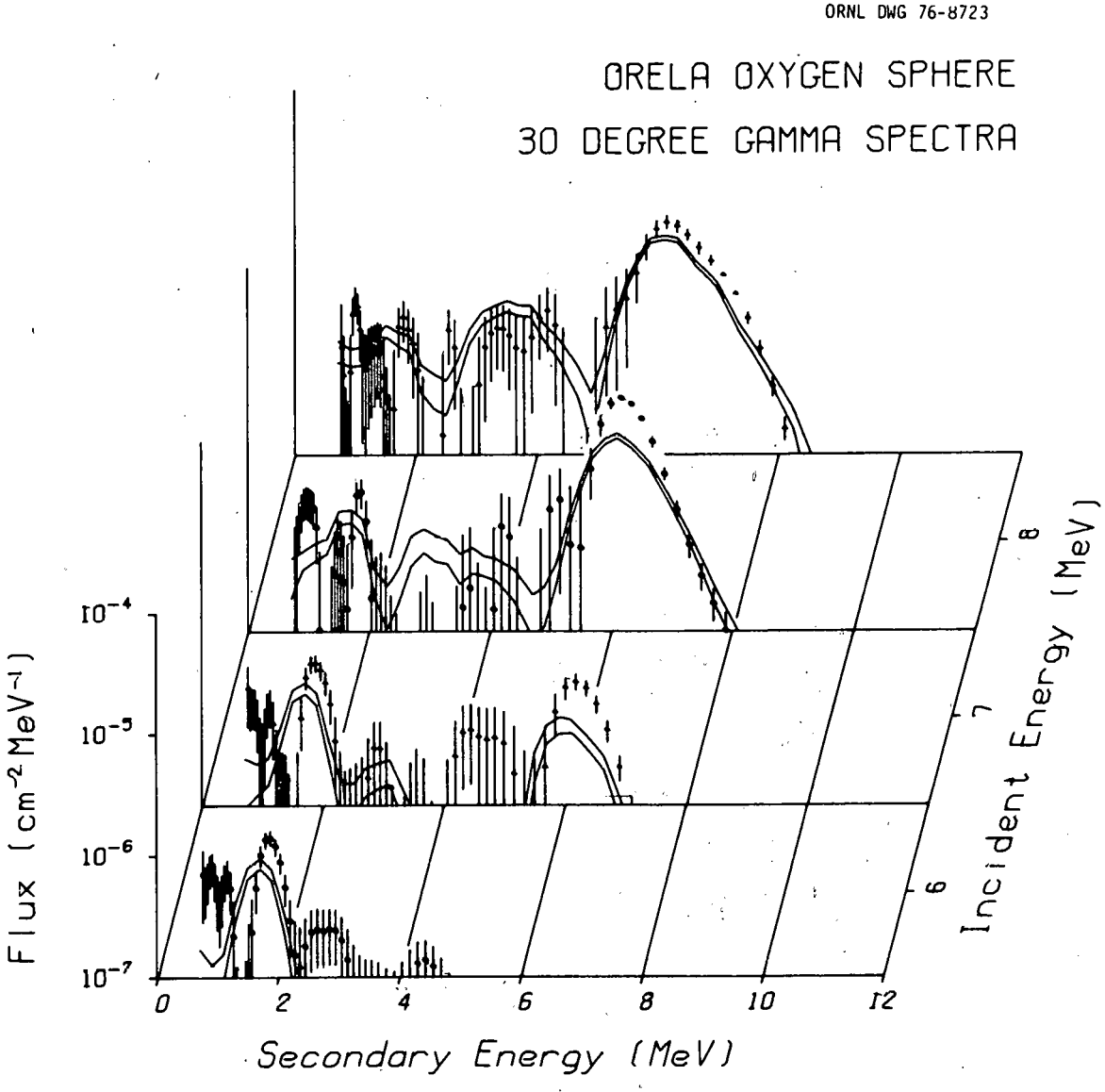

Fig. 21. Secondary Gamma-Ray Spectra Comparisons at 30 deg Using ENDF/B-IV Oxygen Data.

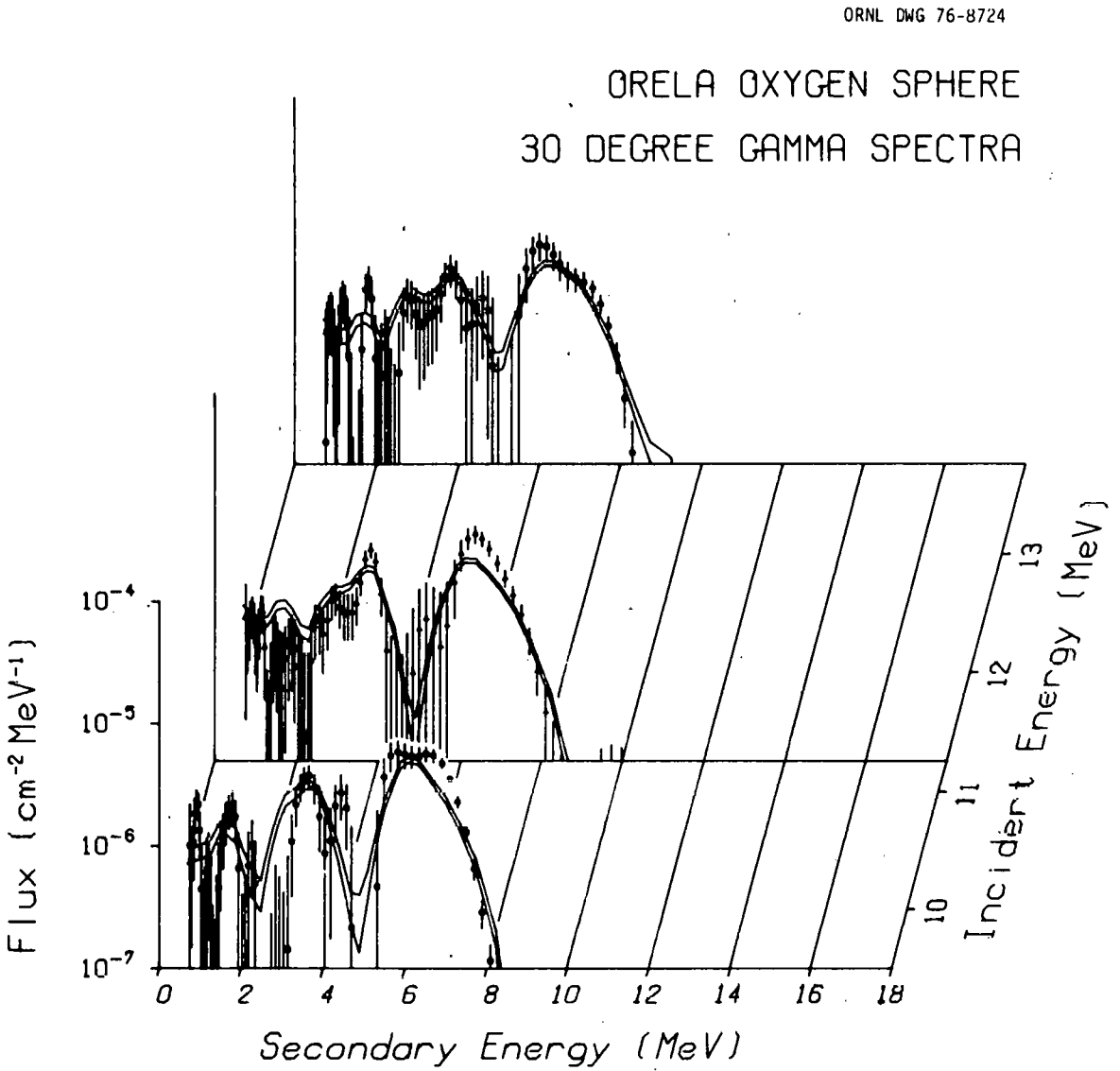

Fig. 22. Secondary Gamma-Ray Spectra Comparisons at 30 deg Using ENDF/B-IV Oxygen Data.

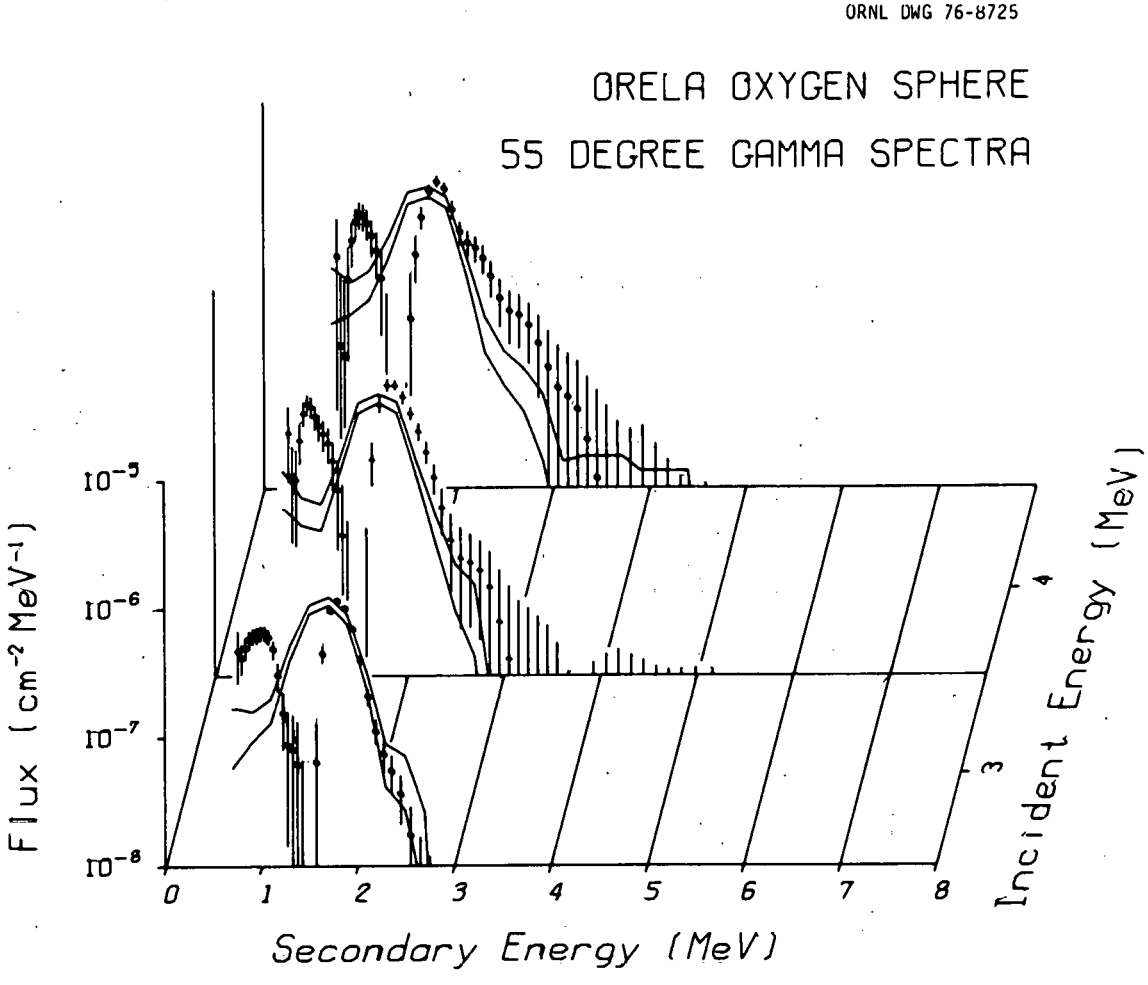

Fig. 23. Secondary Gamma-Ray Spectra Comparisons at 55 deg Using ENDF/B-IV Oxygen Data.

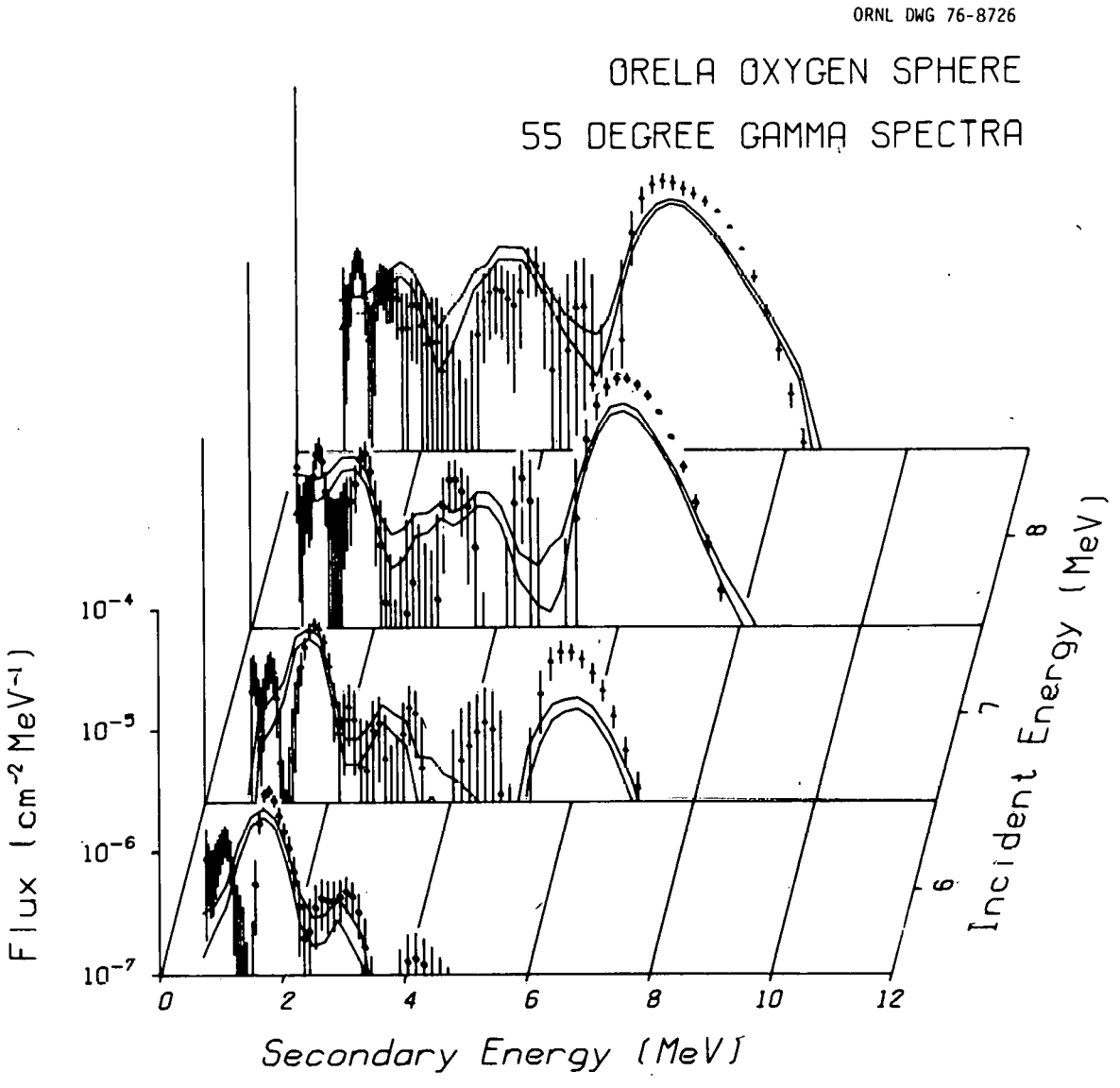

Fig. 24. Secondary Gamma-Ray Spectra Comparisons at 55 deg Using ENDF/B-IV Oxygen Data.

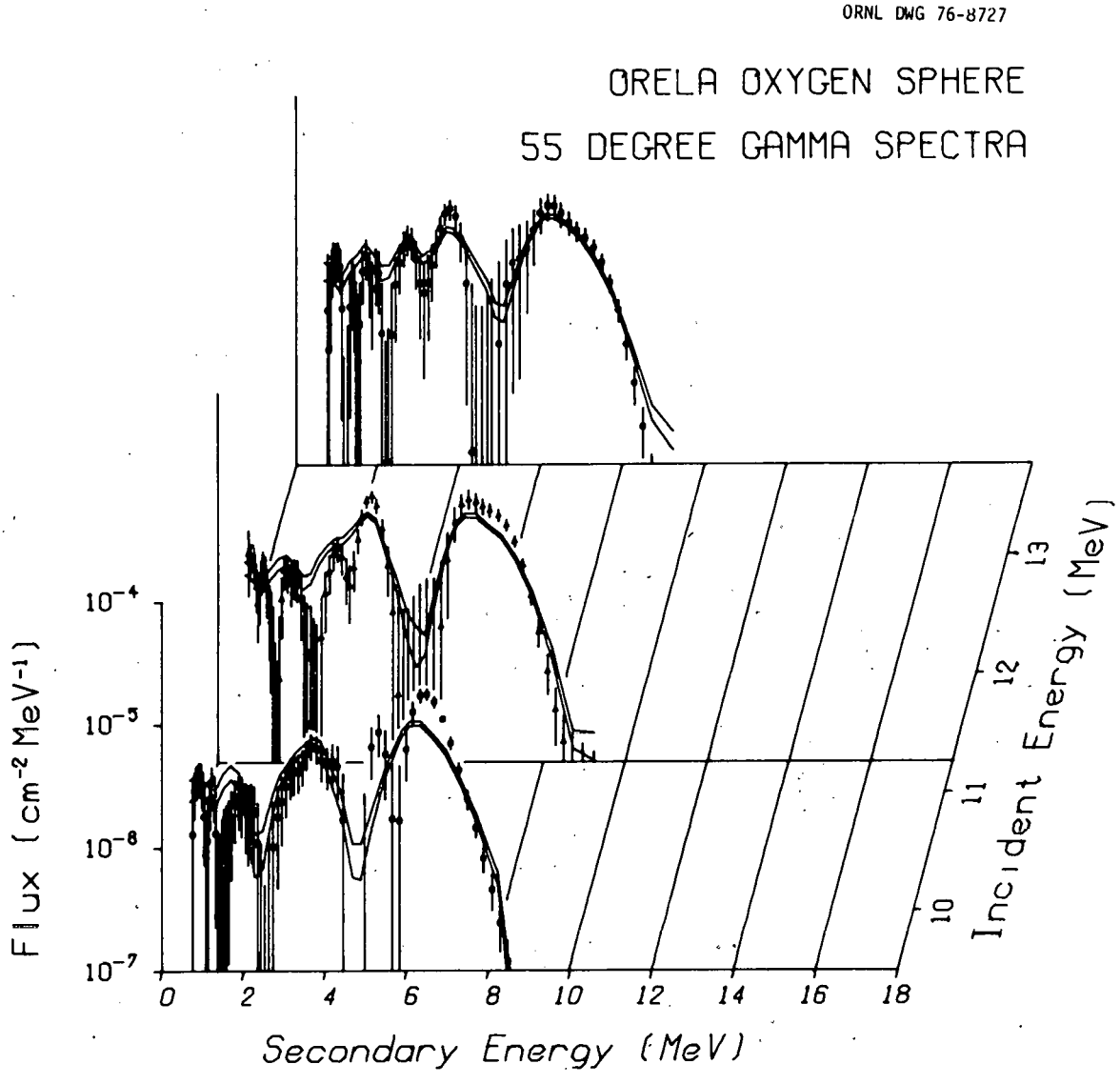

Fig. 25. Secondary Gamma-Ray Spectra Comparisons at 55 deg Using ENDF/B-IV Oxygen Data.

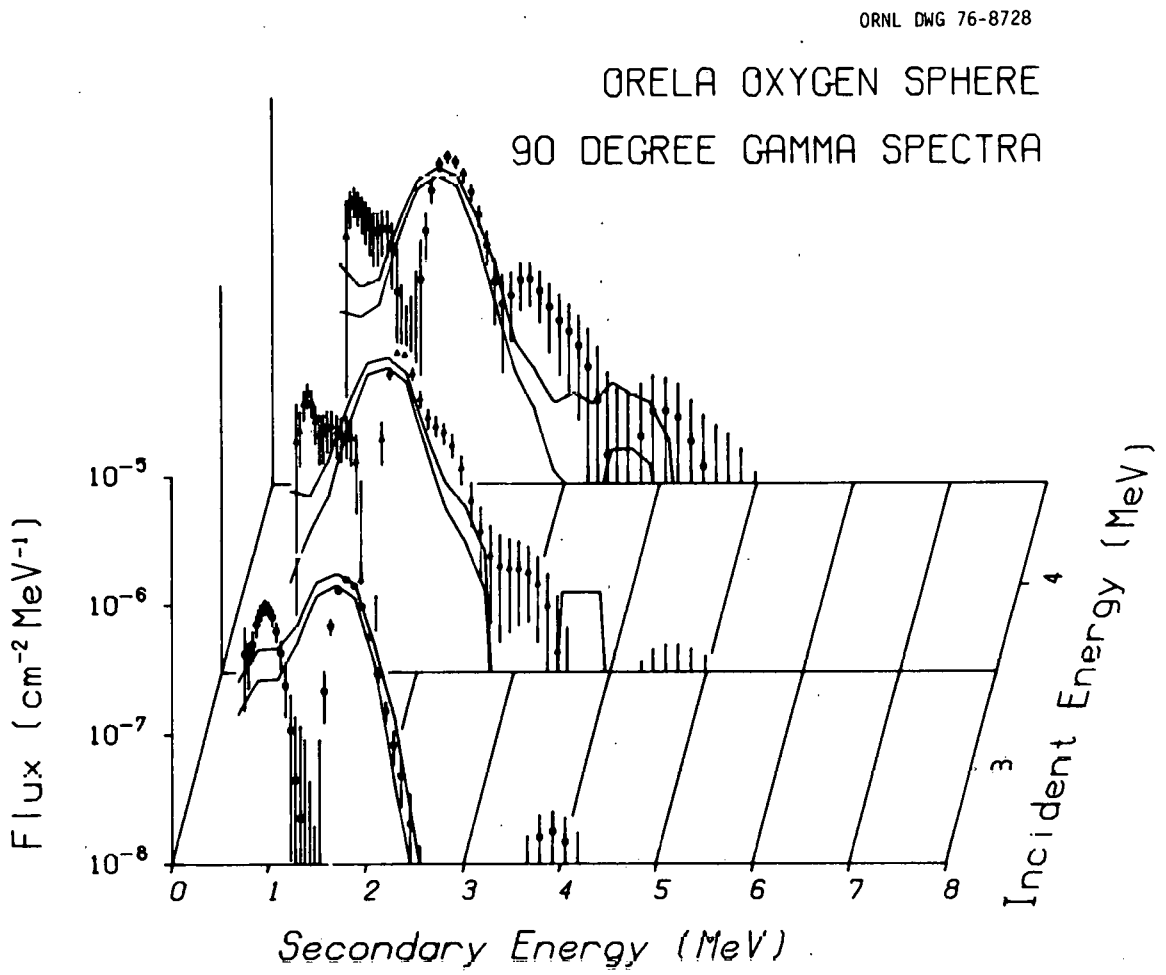

Fig. 26. Secondary Gamma-Ray Spectra Comparisons at 90 deg Using ENDF/B-IV Oxygen Data.

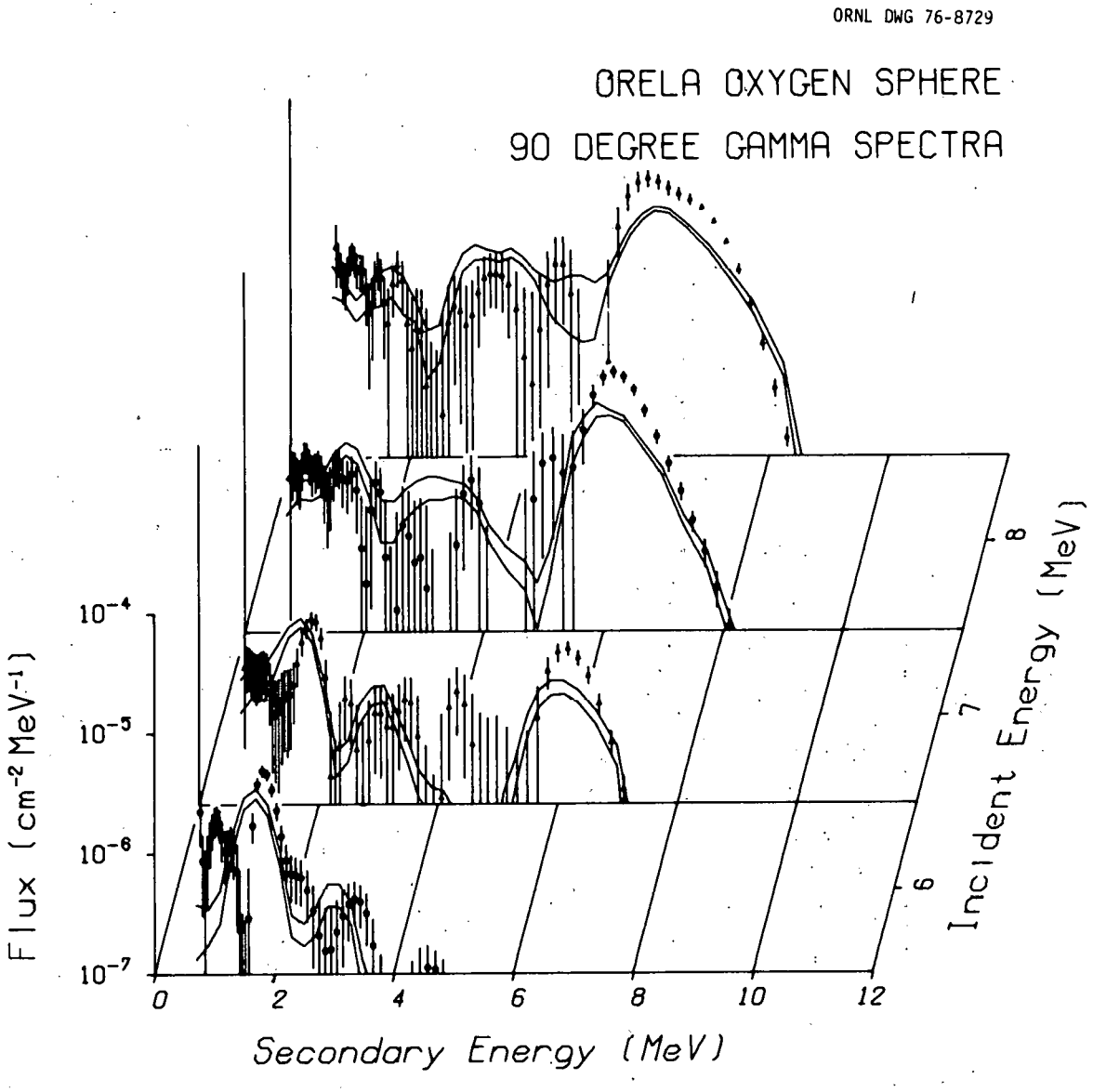

Fig. 27. Secondary Gamma-Ray Spectra Comparisons at 90 deg Using ENDF/B-IV Oxygen Data.

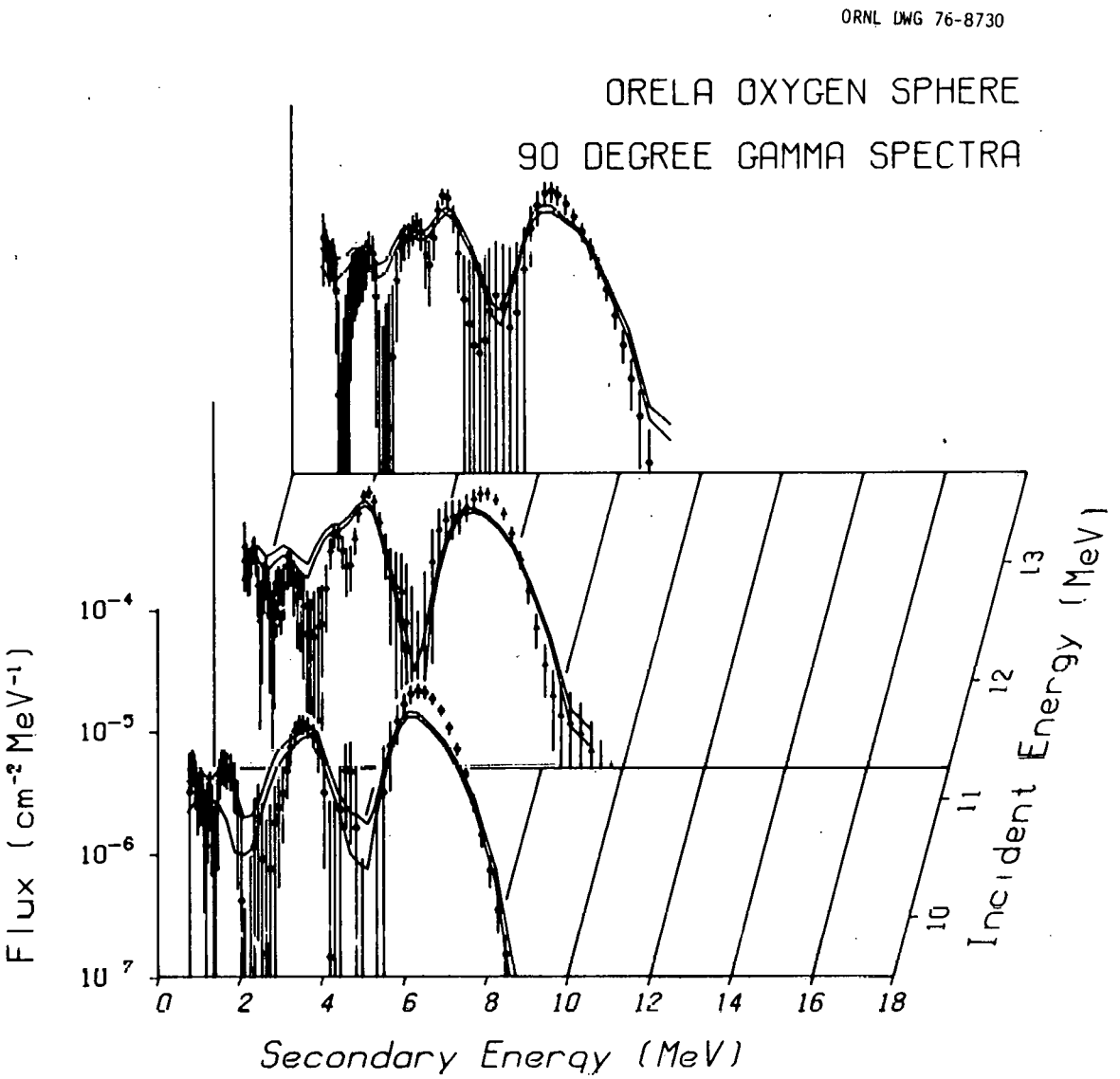

Fig. 28. Secondary Gamma-Ray Spectra Comparisons at 90 deg Using ENDF/B-IV Oxygen Data.

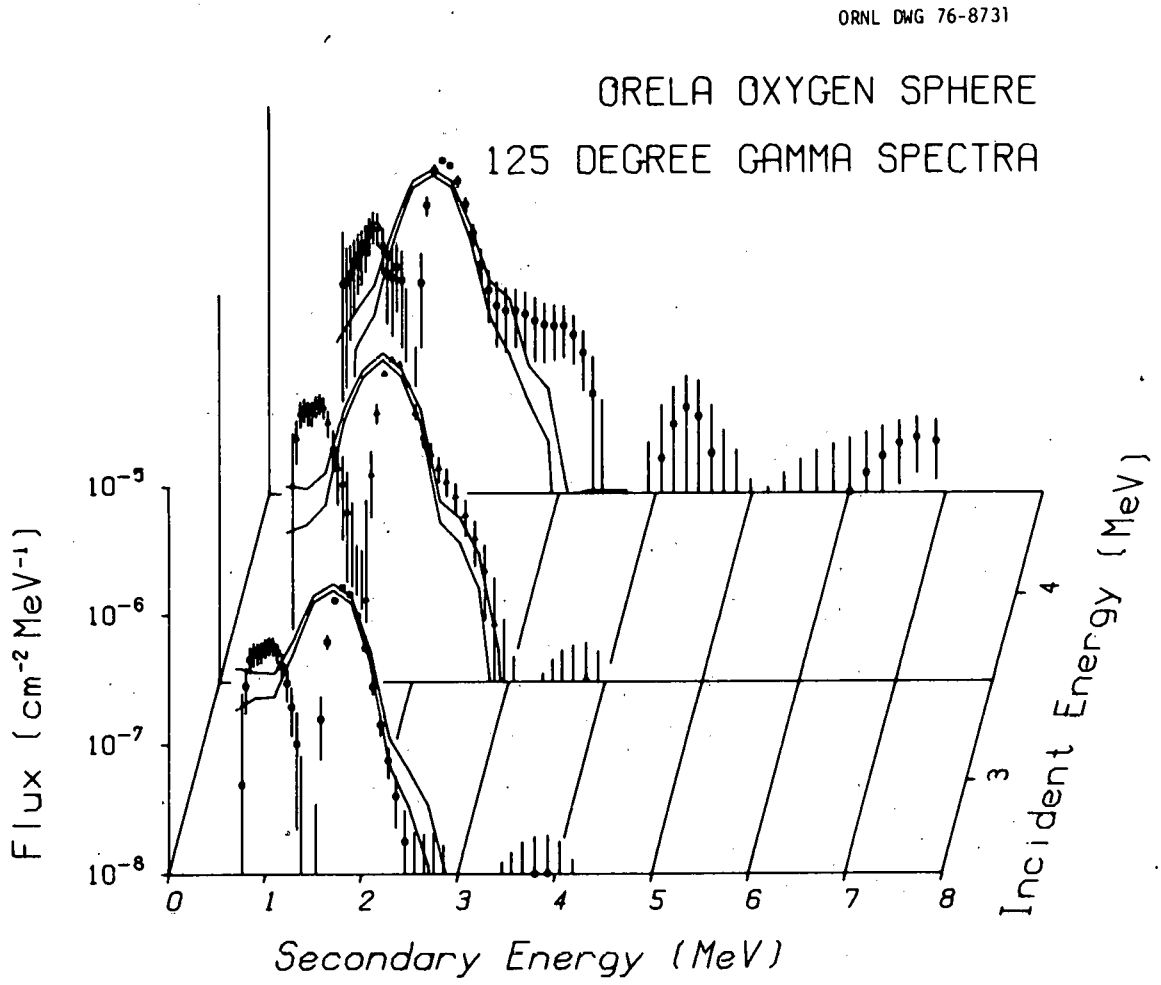

Fig. 29. Secondary Gamma-Ray Spectra Comparisons at 125 deg Using ENDF/B-IV Oxygen Data.

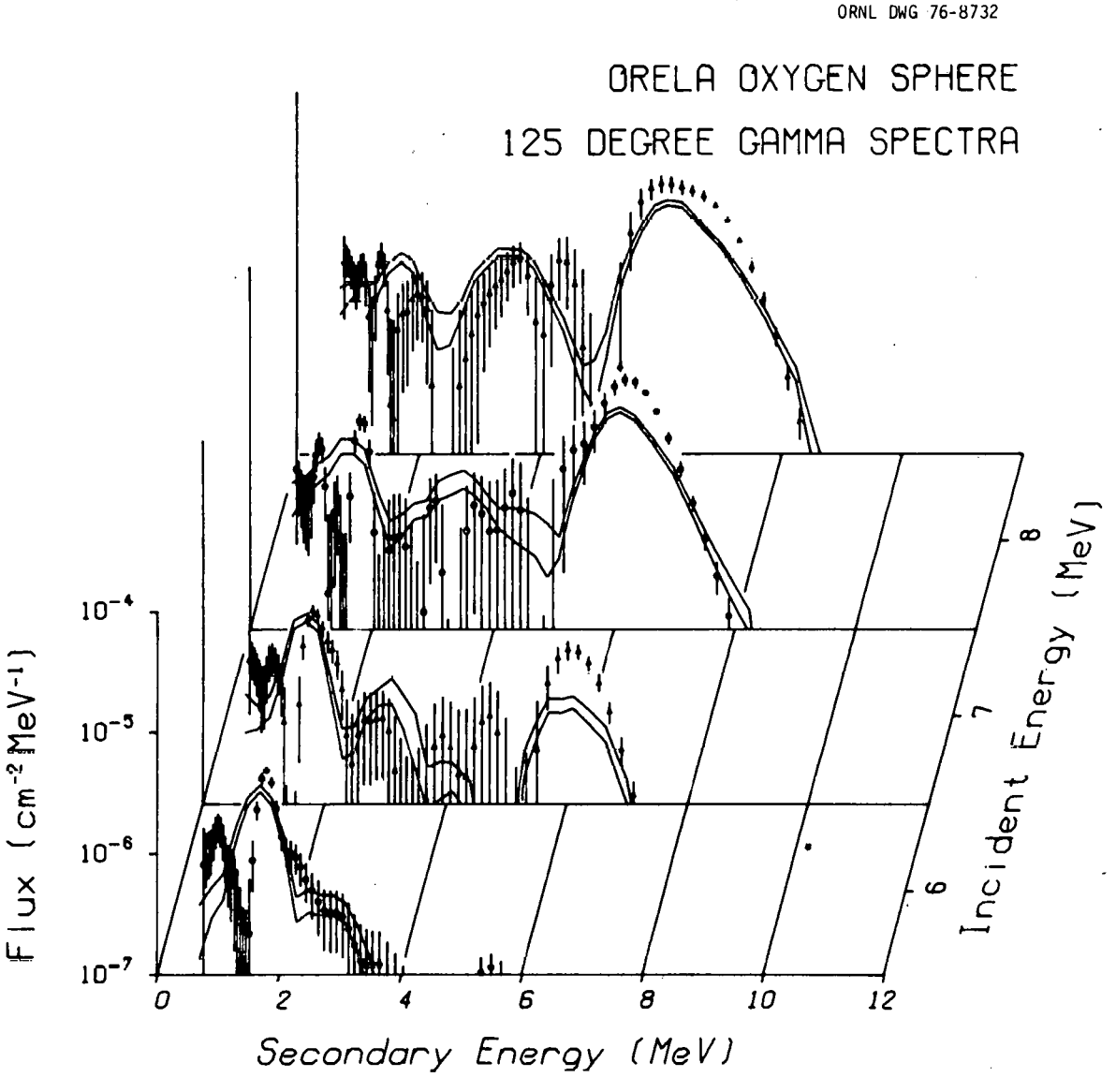

Fig. 30. Secondary Gamma-Ray Spectra Comparisons at 125 deg Using ENDF/B-IV Oxygen Data.

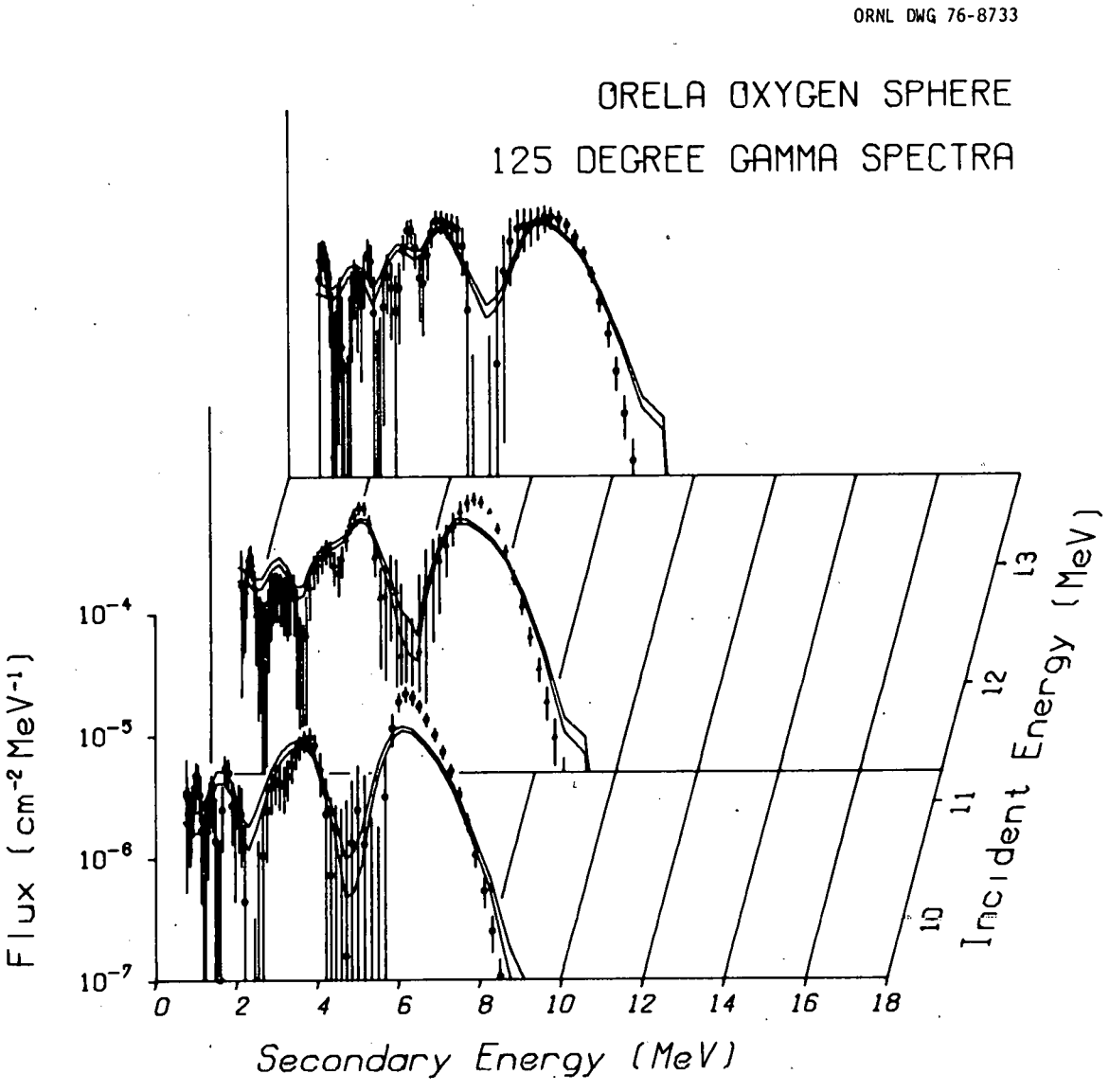

Fig. 31. Secondary Gamma-Ray Spectra Comparisons at 125 deg Using ENDF/B-IV Oxygen Data.

References

1. G. L. Morgan, "Measurement of Secondary Neutrons and Gamma Rays Produced by Neutron Interaction with Nitrogen and Oxygen Over the Incident Energy Range 1 to 20 MeV," Oak Ridge National Laboratory report ORNL-TM-5023 (1975).

2. G. L. Morgan, T. A. Love, and F. G. Perey, "An Experimental System for Providing Data to Test Evaluated Secondary Neutron and Gamma-Ray Production Cross Sections Over the Incident Neutron Energy Range from 1 to 20 MeV," Nucl. Instr. & Meth., 128, 125 (1975).

3. S. N. Cramer and E. M. Oblow, "Analyses of Neutron Scattering and Gamma-Ray Production Integral Experiments on Carbon for Neutron Energies from 1 to 15 MeV," Oak Ridge National Laboratory report ORNL-TM-4494 (1974); see also Nucl. Sci. Eng., 58, 33 (1975).

4. S. N. Cramer and E. M. Oblow, "Analysis of Neutron Scattering and Gamma-Ray Production Integral Experiments on Nitrogen for Neutron Energies from 1 to 15 MeV," Oak Ridge National Laboratory report ORNL-TM-5220 (1976).

5. M. B. Emmett, "The MORSE Monte Carlo Radiation Transport Code System," Oak Ridge National Laboratory report ORNL-4972 (1975).

6. R. W. Roussin, "The Defense Nuclear Agency Working Cross Section Library - Description and Contents," Oak Ridge National Laboratory (Radiation Shielding Information Center) report ORNL-RSIC-34 (1972).

7. N. M. Greene et al., "AMPX - A Modular Code System to Generate Coupled Multigroup Neutron-Gamma Cross Sections from ENDF/B," Oak Ridge National Laboratory report ORNL-TM-3706 (1976).

8. D. E. Bartine, E. M. Oblow, and F. R. Mynatt, "Radiation Transport Cross-Section Sensitivity Analysis - A General Approach Illustrated for a Thermonuclear Source in Air," Nucl. Sci. Eng. 55, 147 (1974).

9. D. G. Foster, Jr., and P. G. Young, "A Preliminary Evaluation of the Neutron and Photon Production Cross Sections for Oxygen," LA-4780, Los Alamos Scientific Laboratory (1972); see also, D. Garber, "ENDF/B Summary Documentation," ENDF-201, National Neutron Cross Section Center (1975).

10. D. E. Bartine et al., "Sensitivity Studies of Concrete Shielded Missile Silos," unpublished ORNL report, private communication (1975); see also, D. E. Bartine, J. V. Pace, III, and J. R. Knight, "A Cross-Section Sensitivity Study of Radiation Transport in Concrete," Trans. Am. Nucl. Soc., 18, 381 (1974).

Internal Distribution

1. L. S. Abbott
2. R. G. Alsmiller, Jr.
3. D. E. Bartine
4. C. E. Clifford
5-9. S. N. Cramer
10. J. K. Dickens
11. C. Y. Fu
12. H. Goldstein (consultant)
13. W. E. Kinney
14. D. C. Larson
15. T. A. Love
16. R. E. Maerker
17. F. C. Maienschein
18. G. L. Morgan
19. F. R. Mynatt
20-24. E. M. Oblow
25. R. W. Peelle
26. F. G. Perey
27. R. W. Roussin
28. M. L. Tobias
29. C. R. Weisbin
30. A. Zucker
31. P. F. Fox (consultant)
32. W. W. Havens, Jr. (consultant)
33. A. F. Henry (consultant)
34. R. E. Uhrig (consultant)
35-36. Central Research Library
37. ORNL Y-12 Technical Library Document Reference Section
38. Laboratory Records Department
39. Laboratory Records ORNL RC
40. ORNL Patent Office
41-42. Radiation Shielding Information Center

External Distribution

43. ERDA Oak Ridge Operations, Research and Technical Support Division, P. O. Box E, Oak Ridge, TN 37830: Director
44-70. Technical Information Center
71-144. Given special NPD DNA distribution